Master of Science in Petroleum Engineering

2022

Master Thesis

CO_2 Injection and Storage in Deep Saline Aquifers: Sensitivities on Model Gridding and Geochemistry

Supervisor:

Prof. Francesca VERGA

Candidate:

Alessandro SURIANO

Abstract

Geological carbon dioxide sequestration and underground storage offer a promising solution to reduce greenhouse gases in the atmosphere. However, technical feasibility and safety issues must be duly addressed.

3D numerical models of potential underground storages to perform compositional simulations of the system dynamic behavior are a way to study the storage of carbon dioxide in existing deep geological formations. After a brief literature review on the CO2 trapping mechanisms when CO2 is injected in deep saline aquifers and on current CCS projects, the thesis focuses on how to set up representative models and obtain reliable simulation results. The task requires the definition of a large set of parameters describing the fluid and the rock properties as well as the rock-fluid interaction properties, but also consideration on how to perform the simulations.

Thus, a synthetic model of a deep saline aquifer was set up and a large number of simulations were performed to investigate the impact of model gridding, CO2 injection strategy and parameters characterizing the system. Real data taken from the literature were used for the sensitivity analyses. The outcomes of the investigations were examined in terms of induced pressure variations, CO2 plume distribution and quantity of trapped CO2 according to the different trapping mechanisms. Results provided a very interesting and novel insight about the need for fine grids especially where the injection wells are located and for the definition of a suitable CO2 injection strategy. They also confirmed the need for a thorough characterization of the rock and formation water composition controlling the geochemical effects and for the rock-fluid interaction properties controlling the capillary trapping.

Index

List of figures

List of tables

Components and minerals

Al^{3+} – Aluminium cation
$Al(OH)_4^-$ – Aluminate
$Al_2Si_2O_5(OH)_4$ – Kaolinite
CO_2 – Carbon dioxide
CO_3^{2-} – Carbonate
$CaAl_2Si_2O_8$ – Anorthite (Feldspar)
$CaCO_3$ – Calcite
$CaCl^+$ – Calcium chloride
$CaHCO_3^-$ – Calcium bicarbonate
$CaMg_{0.3}Fe_{0.7}(CO_3)_2$ – Ankerite
$CaSO_3$ – Anhydrite
$CaSO_4(2H_2O)$ – Gypsum
$CaSiO_3$ – Wollastonite
Cl^- – Chloride ion
Fe^{2+} – Iron cation
$FeCO_3$ – Siderite
FeS_2 – Pyrite
$Fe_2Al_2SiO_5(OH)_4$ – Chamosite-7A (Chlorite)
Fe_2SiO_4 – Fayalite (Olivine)
H^+ – Hydrogen ion
HCO_3^- – Bicarbonate (Hydrogen carbonate)
HS^- – Bisulfide
H_2CO_3 – Carbonic acid
H_2O – Water
K^+ – Potassium cation
$KAlSi_3O_8$ – K-feldspar (Feldspar)
$KAl_3(OH)_6(SO_4)_2$ – Alunite
Mg^{2+} – Magnesium cation
$MgCO_3$ – Magnesite
$MgCaSi_2O_6$ – Diopside
$MgCl^+$ – Magnesium chloride
$MgHCO_3^-$ – Magnesium bicarbonate
Mg_2SiO_4 – Forsterite (Olivine)
$Mg_{2.5}Fe_{2.5}Al_2Si_3O_{10}(OH)_8$ – Chlorite
$Mg_3Fe_3Si_4O_{10}(OH)_8$ – Serpentine
Na^{2+} – Sodium cation
$NaAlCO_3(OH)_2$ – Dawsonite
$NaAlSi_3O_8$ – Albite (Feldspar)
NaCl – Halite
OH^- - Hydroxide ion
SO_4^{2-} – Sulfate
SiO_2 – Chalcedony (Quartz)

1. Introduction

1.1 Carbon Capture and Storage

Nowadays, humanity is facing one of the biggest challenges that Earth has ever lived through: climate change due to the accumulation of Greenhouse Gases (GHG) in the atmosphere. Since carbon dioxide gives one of the most important contributions to GHG, reducing its emission is considered one of the main steps to limit GHG. Carbon dioxide is, along with water, the main product of oxidation reactions and it is generated by numerous processes which involve power generation, oil and gas processing, production of cement, iron, steel and glass. Since the products of these processes are vitally important to the industry and technology development and their demand worldwide is increasing year after year, it is not possible to consider limiting them as a solution to carbon dioxide emissions. Here it comes the importance of considering a negative emission technology such as Carbon Capture and Storage (CCS) [1-8], which was firstly introduced in a theoretical way at the end of XX century and then started to be developed in real fields during the first part of the current century. CCS now represents one of the most significant and promising solutions to reach a Net-Zero Emissions scenario by 2050. IEA's sustainable development scenario delivering a 66% probability of limiting global temperature rise to 1.8°C without large-scale negative emissions includes a 9% emissions reduction from CCUS; to reach this target the average mass of CO_2 that needs to be captured and permanently stored each year before 2050 is 1.5 GT/yr (with an annual storage expected to be 2.5 GT/yr by 2050) [9].

CCS simply consists in capturing the carbon dioxide both as a process product or directly from the atmosphere and injecting it in feasible underground geological formations which should fulfill the following conditions: the capacity to store an adequate volume of CO_2, the ability to accept the injected CO_2 at the rate that it is supplied, the ability to contain the CO_2 plume by the overlying layers and the existence of a sufficiently stable geological setting to avoid compromising the integrity of the storage site and stability [10-11]. To be stored, CO_2 is generally transported and injected in de-hydrated supercritical phase; thus, temperature must be higher than 31 °C and pressure must be higher than 73 bar. These temperature and pressure conditions are generally achieved in formations deeper than approximately 1000 m [12]. The significant advantage of injecting CO_2 in supercritical phase is its liquid-like density that provides the potential for efficient utilization of underground storage space in the pores of sedimentary rocks [13].
Hydrodynamic flow and geochemical phenomena, triggered by the alteration of the geochemical equilibrium between the porous rocks and the formation water when massive quantities of CO_2 are injected into aquifers, coupled to the thermodynamic conditions of the storage site can favor the development of different trapping mechanisms [13-16]. They are conventionally divided into hydrogeological and geochemical mechanisms [17].

1.2 Hydrogeological trapping mechanisms

- Stratigraphic and structural trapping

When it is injected in a permeable geological trap closure, which could be either an anticline, a fault seal, a stratigraphic pinchout or an unconformity, CO_2 tends to migrate upward because of the density gradient

until it reaches a low-permeability layer defined as caprock. Once supercritical CO_2 reaches the caprock it tends to flow laterally, forming a free phase plume. The extension of the plume depends on the injected quantity of CO_2 and on the main properties and heterogeneities of the formation. This mechanism is defined as stratigraphic and structural trapping (Figure 1) and it is the most significant trapping mechanism when CO_2 is injected in depleted gas reservoirs. The quantity of CO_2 trapped in this way is limited by the geometry of the stratigraphic or structural trap designed as carbon storage. The safety level of this storage relies on the caprock integrity. There are four different ways in which the caprock can fail: diffusive losses through the caprock, leakage through pore spaces when capillary breakthrough pressure has been exceeded, leakage through faults or fractures, and well leakage when well completions are degraded or inappropriately abandoned [18]. Another issue that can alter the storage safety is represented by the possibility of CO_2 lateral spilling, this happens when the CO_2 plume is so extended and deep that it flows below the closure spill point; to avoid that, accurate assessment of the depth of the spill point must be made.

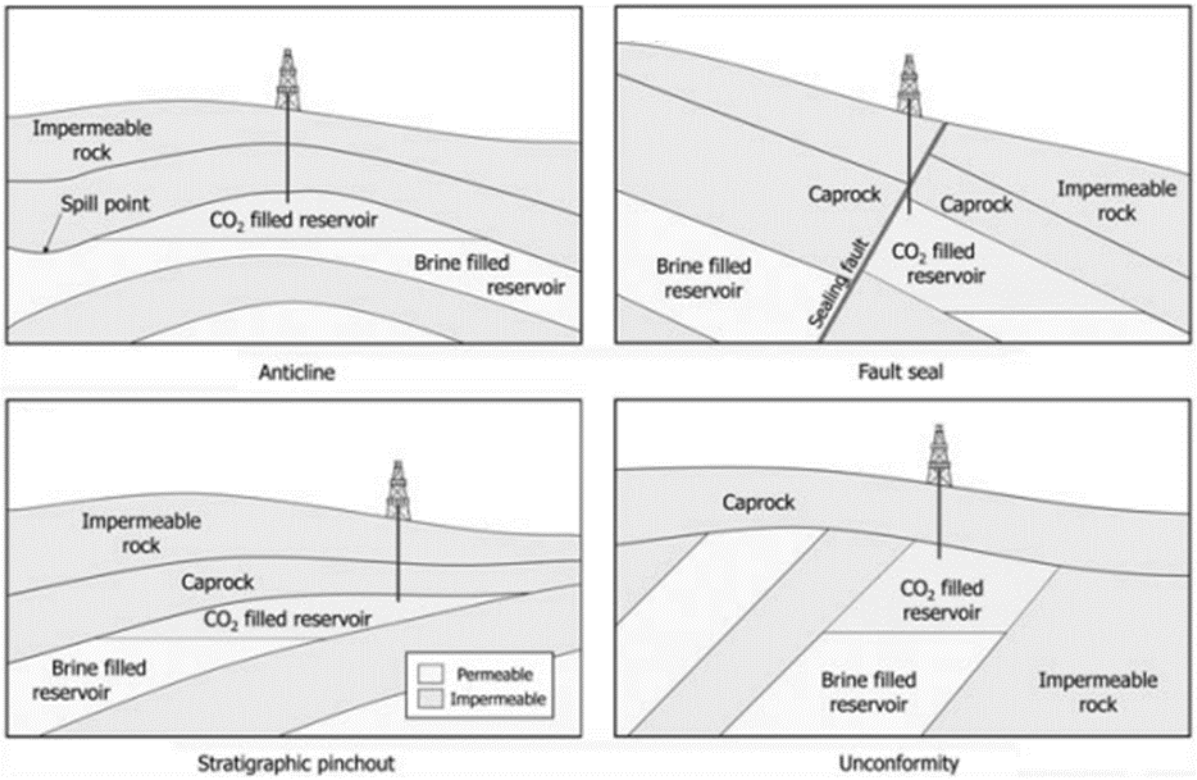

Figure 1 *Stratigraphic/structural trapping of CO_2 in different closure features [19]*

- Hydrodynamic trapping

Hydrodynamic trapping (Figure 2) is similar to stratigraphic and structural trapping with the exception that it does not take place in a closed reservoir but in an open saline aquifer overlaid by a caprock layer characterized by a gentle dip. When the CO_2 reaches the caprock, it flows along it and starts moving up to the surface with a slow and controlled velocity. Its spreading velocity and final plume extension depend on many factors, such as the dip of the caprock, the heterogeneities in the aquifer and the aquifer flow velocity.

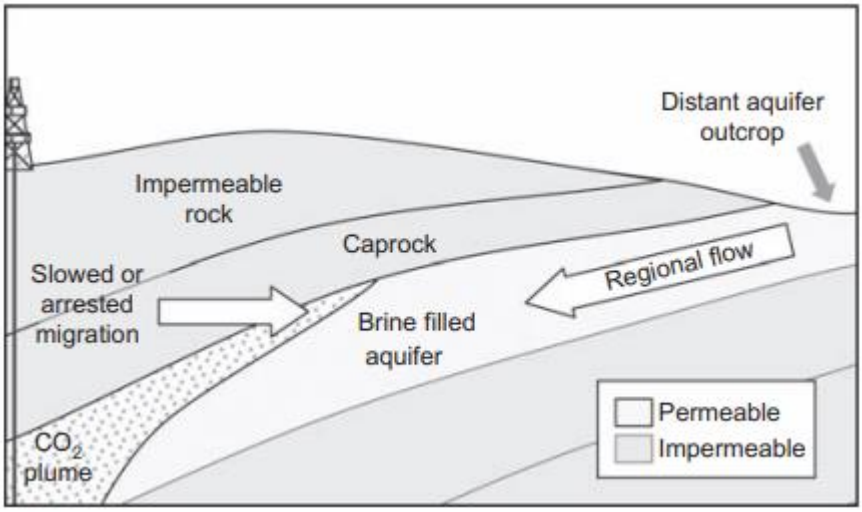

Figure 2 *Hydrodynamic trapping of CO_2 [19]*

- Residual trapping

Residual trapping occurs when brine replaces the volume previously occupied by the injected CO_2, which is thus permanently trapped by capillary forces as free-phase disconnected droplets (Figure 3). By definition, CO_2 is residual trapped only when injection finishes and the CO_2 plume migrates upward or laterally. The amount of carbon dioxide that is residual trapped depends on the path of CO_2 plume and on the fluid-rock interaction properties, namely on the residual saturation of CO_2 after water imbibition occurs; the higher is this value, the larger the quantity of CO_2 that can be trapped by capillary forces as it travels through the formation. Different curves for drainage and imbibition processes apply due to hysteresis and many models such as Land [20], Carlson [21], and Aissaoui [22] are able to predict the residual saturation of CO_2.

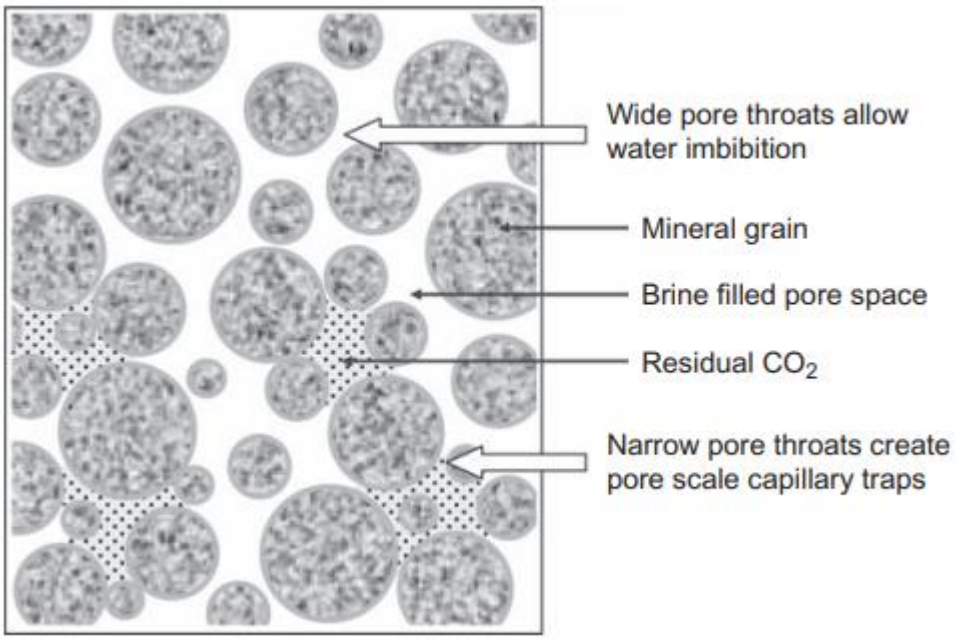

Figure 3 *Residual trapping of CO2 following plume migration [19]*

Relative permeability curves based on Land model (Figure 4) can help to describe hysteresis: once CO_2 saturation reaches the critical value S_{gcrit}, CO_2 relative permeability increases along the drainage curve as a function of the CO_2 saturation increase (CO_2 is injected and displaces the brine). The maximum value that relative permeability can reach is corresponding to the maximum possible saturation of CO_2, which is equal to $1-S_{wcon}$, where S_{wcon} is the irreducible (or connate) water saturation . When CO_2 injection stops and it is replaced by brine in the pores it previously occupied, CO_2 relative permeability follows a linear imbibition curve (uniquely based on S_{gh} which is the saturation that CO_2 reached at the end of the drainage) to become zero at the saturation value S_{grh}, which is the residual saturation of CO_2 considering relative permeability hysteresis.

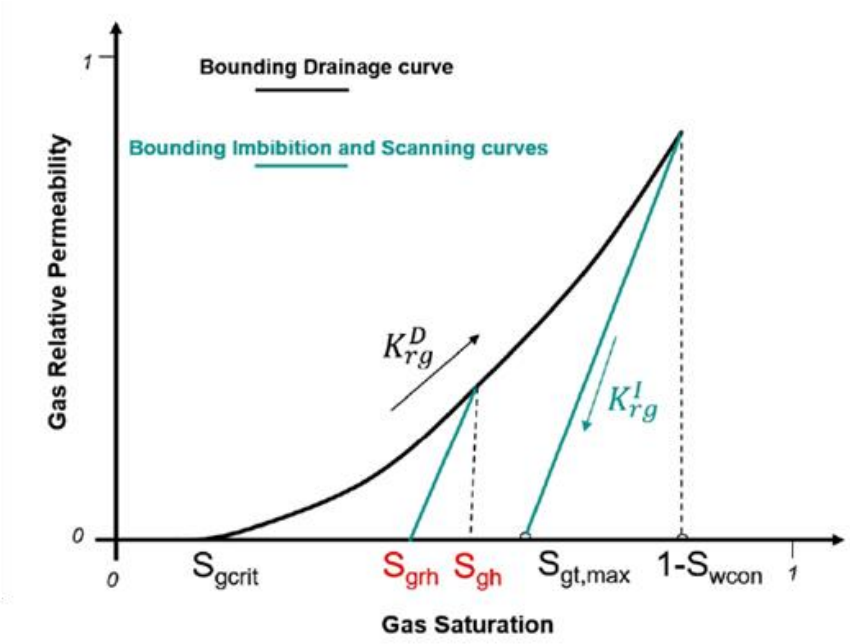

Figure 4 *Saturation hysteresis based on Land [20] model*

1.3 Geochemical trapping mechanisms

- Solubility trapping

Once supercritical CO_2 is injected in the subsurface it exists as a free phase plume. CO_2 at the plume interface interacts with the formation brine and dissolves into it according to the reaction:

$$CO_2 + H_2O \leftrightarrow H_2CO_3$$

(1) Dissolution of carbon dioxide in water (Carbonic acid formation)

Solubility of carbon dioxide in water increases with pressure but decreases with temperature and water salinity. Even though the kinetics of CO_2 dissolution is extremely fast, the dissolution of the injected CO_2 is a rather slow process: only a fraction of the injected volume is sequestered due to aqueous solubility over hundreds of years [23].

Since brine containing dissolved CO_2 is denser than the original formation brine, thus it tends to sink and be replaced by fresh brine (without dissolved CO_2). This natural fluid mixing enhances the dissolution of CO_2 and makes solubility trapping a mechanism characterized by a high level of safety. Carbon dioxide moves into the aqueous phase also due to diffusivity but with a velocity much slower than the one of convective mixing. However, diffusivity must be duly addressed because it is defined as one of the possible leaking phenomenon through the sealing caprock [18].

- Ionic trapping

Carbonic acid, formed by dissolution of pure carbon dioxide into brine, is a weak acid and, depending on the availability of hydroxide ions, it forms bicarbonate and carbonate ions through the reactions:

$$H_2CO_3 + OH^- \leftrightarrow H_2O + HCO_3^-$$

(2) Dissociation of carbonic acid in bicarbonate

$$HCO_3^- + OH^- \leftrightarrow H_2O + CO_3^{2-}$$

(3) Dissociation of bicarbonate in carbonate ion

The amount of CO_2 trapped by ionic trapping is strongly dependent on the quantity of CO_2 already dissolved in the brine and on the brine pH which governs the dissociation reactions (2) and (3). According to the qualitative representation in Figure 5, CO_2 exists in the form of carbonate ions for high pH of the formation brine (basic environment), in the form of bicarbonate for medium pH (neutral environment) and in the form of carbonic acid for low pH (acid environment).

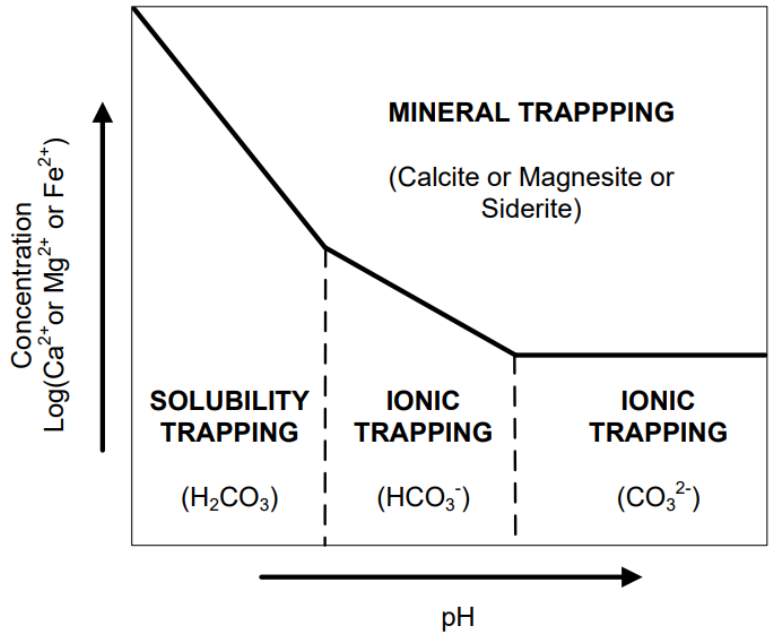

Figure 5 *Geochemical trapping mechanisms dependency on brine pH and metal cations concentration [24]*

Ionic trapping is fundamental to trigger mineral trapping because carbonate ions and bicarbonate are much more unstable and reactive than carbonic acid when they interact with dissolved cations to form precipitates.

- Mineral trapping

Mineral trapping is the geochemical mechanism which guarantees the highest level of safety. CO_2 is mineral trapped when it reacts with non-carbonate mineral derived metal cations and it precipitates in the form of carbonate minerals. The high safety is given by the fact that, once they have precipitated, carbonate minerals are extremely stable and so CO_2 remains permanently trapped as a solid phase. Main mineral reactants and products are summarized in Figure 6.

Mineral reactants		**Molecular weight**	**Specific gravity**	**Potential CO_2 fixed**	
				kg/kg mineral	**kg/m^3 mineral**
Olivine					
Forsterite	Mg_2SiO_4	140.7	3.2–3.3	0.62	2020
Fayalite	Fe_2SiO_4	203.8	4.39	0.43	1890
Diopside	$MgCaSi_2O_6$	216.6	3.3–3.6	0.41	1400
Wollastonite	$CaSiO_3$	116.2	2.9–3.1	0.38	1140
Chlorite	$Mg_{2.5}Fe_{2.5}Al_2Si_3O_{10}(OH)_8$	602.7	2.6–3.3	0.37	1080
Serpentine	$Mg_3Fe_3Si_4O_{10}(OH)_8$	648.9	2.2–2.9	0.41	1040
Feldspars					
Albite	$NaAlSi_3O_8$	262.3	2.63	0.17	440
Anorthite	$CaAl_2Si_2O_8$	278.2	2.74	0.16	430
K-feldspar	$KAlSi_3O_8$	278.4	2.59	0.16	410

Reaction products			
Calcite	$CaCO_3$	Dawsonite	$NaAlCO_3(OH)_2$
Magnesite	$MgCO_3$	Ankerite	$CaMg_{0.3}Fe_{0.7}(CO_3)_2$
Siderite	$FeCO_3$	Alunite	$KAl_3(OH)_6(SO_4)_2$
Anhydrite	$CaSO_4$	Chalcedony	SiO_2
Gypsum	$CaSO_4 \cdot 2H_2O$	Kaolinite	$Al_2Si_2O_5(OH)_4$

Figure 6 *Typical mineral trapping reactants and reaction products [25]*

Typical mineral reactions associated to mineral trapping [25] are:

$$2NaAlSi_3O_8 + H_2CO_3 + H_2O + Ca^{2+} \leftrightarrow 4SiO_2 + CaCO_3 + Al_2Si_2O_5(OH)_4 + 2Na^+$$

(4) Precipitation of calcite and kaolinite from the carbonation of albite

$$NaAlSi_3O_8 + H_2CO_3 \leftrightarrow 3SiO_2 + NaAlCO_3(OH)_2$$

(5) Precipitation of dawsonite from the carbonation of albite

$$CaAl_2(SiO_4)_2 + CO_2 + 2H_2O \leftrightarrow CaCO_3 + Al_2Si_2O_5(OH)_4$$

(6) Precipitation of calcite and kaolinite from the carbonation of anorthite

$$KAlSi_3O_8 + CO_2 + H_2O + Na^+ \leftrightarrow 3SiO_2 + NaAlCO_3(OH)_2 + K^+$$

(7) Precipitation of dawsonite from the carbonation of K-feldspar

$$Mg_{2.5}Fe_{2.5}Al_2Si_3O_{10}(OH)_8 + 2.5CaCO_3 + 5CO_2 \leftrightarrow 2.5FeCO_3 + 2.5MgCa(CO_3)_2 + Al_2Si_2O_5(OH)_4 + SIO_2 + 2H_2O$$

(8) Precipitation of siderite, dolomite and kaolinite from the alteration of clay mineral chlorite

Even if mineral trapping of CO_2 starts as soon as carbon dioxide is solubilized into the formation brine, geological timescales are needed to have a significant amount of CO_2 precipitated in the form of carbonate minerals due to the slowness of these type of geochemical reactions [25-26]. Furthermore, if carbonate minerals (Calcite, Magnesite, Siderite, …) are initially present in the formation, they can be attacked by the weak carbonic acid that forms when injected CO_2 reacts with brine, releasing additional bicarbonate and carbonate ions in the brine. It is important to highlight that rock properties as absolute permeability and porosity may suffer changes in their values in case of significant mineral dissolution or precipitation: carbonate mineral precipitation will decrease the formation porosity and permeability. Conversely, dissolution will increase both these parameters. Should the caprock be subject to carbonate minerals dissolution, its integrity may be compromised.

1.4 Interaction among different trapping mechanisms

Each trapping mechanism is dependent on each other: if CO_2 is not retained in the subsurface in supercritical phase by hydrogeological trapping mechanisms, it cannot dissolve into brine triggering solubility trapping as well as dissociation reactions which in turn activate ionic trapping, and, eventually, CO_2 cannot precipitate as carbonate minerals (mineral trapping) if carbonate and bicarbonate ions are not dissolved into the brine (Figure 7).

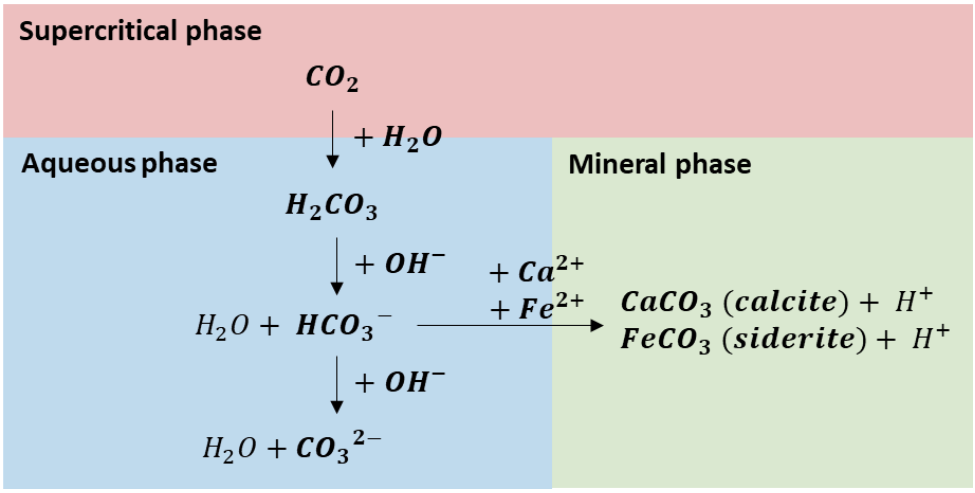

Figure 7 *Example of interaction between physical and geochemical trapping mechanisms*

All trapping mechanisms exist at the same time but the amount of CO_2 that they involve changes over time. During injection, the main trapping mechanism is structural/stratigraphic/hydrodynamic but when the injection ceases and the CO_2 plume migrates, part of the supercritical CO_2 remains trapped in pores by capillary forces activating residual trapping. Even if dissolution and dissociation aqueous reactions are extremely fast and solubility and ionic trapping are triggered as soon as CO_2 is injected, many years

are needed to trap a significant amount of CO_2 in the aqueous phase. Finally, geochemical equilibrium is reached and mineral trapping occurs after thousands of years. Figure 8 shows in a qualitative way how the trapping mechanisms vary as a function of time.

The following also applies [23] as a general "rule of thumb" to represent the mechanisms relative time scale:

$$t_{structural/stratigraphic} < t_{residual} \leq t_{solubility/ionic} \leq t_{mineral}.$$

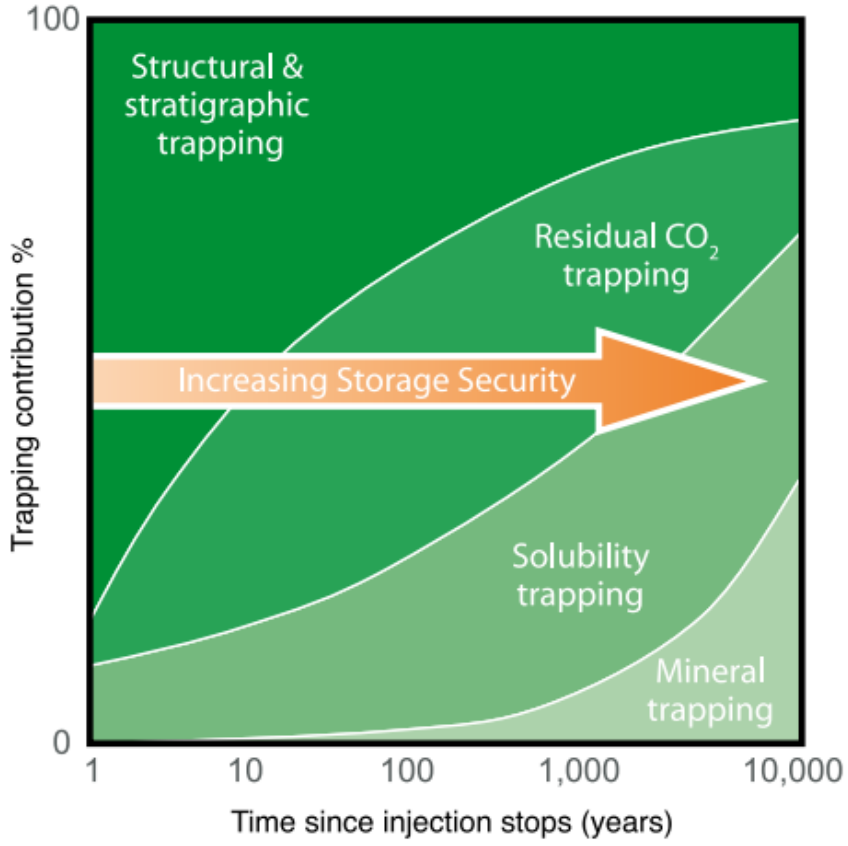

Figure 8 *Trapping mechanisms contribution over time and storage safety [13]*

1.5 Feasible targets for CCS

Main formations feasible for CCS projects can be open saline aquifers, saline aquifer closures, depleted or depleting oil and gas reservoirs [27].

- Open saline aquifers

Injecting CO_2 in open aquifers, monitoring its path and interaction with the formation during and after injection is also called Migration Assisted Storage (MAS). When CO_2 is injected in an open aquifer, its free-phase plume will move towards the caprock and spread under it. The caprock must have a gentle dip in order to activate hydrodynamic trapping mechanism and so control the velocity with which the CO_2 plume moves upward trying to reach the surface. Due to the high extent of the interface between CO_2 and formation brine, the predominant trapping mechanism in MAS is solubility trapping, which will

be significant, in terms of CO_2 trapped, since the early life of the project. Heterogeneities in the target formation are a positive feature since they complicate the path, enhancing the interface between spreading CO_2 and brine thus favoring solubility trapping. When CO_2 injection ceases, the moving free phase plume will float towards the sloping caprock, leaving some droplets trapped by capillary forces at its tail (residual trapping). It is important to also consider the aquifer velocity since it shapes the movement and the final extent of the CO_2 plume (Figure 9).

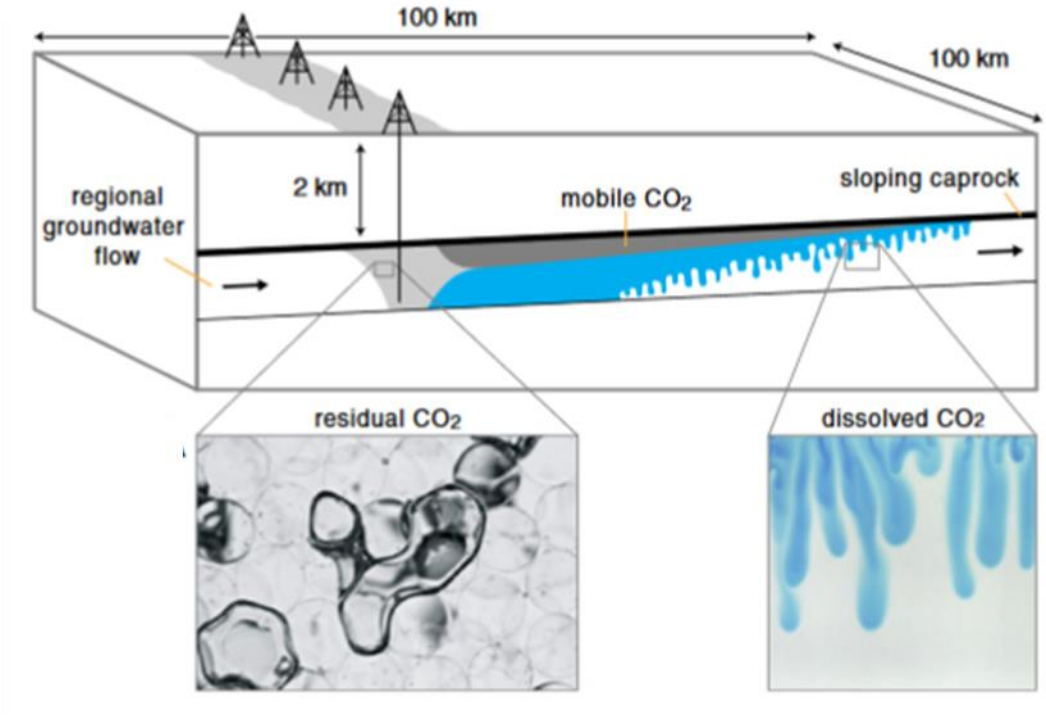

Figure 9 *Trapping mechanisms in MAS [28]*

The main advantage of considering an open aquifer as a CCS target formation is obviously its enormous extent which translates in a potential to store very large volumes of CO_2. The large aquifer volume is also able to absorb any pressure increase due to CO_2 injection, removing any issue related to overpressure, except at the wellbore. However, especially during early injection when CO_2 is building its path through the fully brine saturated formation, a ramp-up injection scenario may be a solution to avoid any possible issue of overpressure even in the near wellbore zone, as it will be discussed in section 4.2. In fact, the injection strategy is a key factor because injection may cause local overpressures able to fracture the formation and even the caprock in the worst case. Besides ramp-up injection also a multi-well scenario can be considered to achieve high injection volumes yet avoiding fractures. However, it was shown that increasing the number of wells decreases the project appeal due to increased costs [29].

One big issue related to large open aquifers relies on uncertainties. Uncertainties about reservoir and caprock suitability and heterogeneity impact the ability to model CO_2 movements effectively; uncertainty about the connectivity with other aquifers can lead to underestimating the risks of leaking paths; and uncertainty on the storage potential may lead to a significant CO_2 volume overestimation. To prevent these problems, an extensive area must be appraised before starting a CO_2 storage project and monitored during and after CO_2 injection.

Miri et al. [30-31], Cui et al. [32] and Tang et al. [33] highlighted the importance of considering salt precipitation when CO_2 is injected into an aquifer characterized by high salinity. CO_2 is transported and injected as dehydrated supercritical fluid to avoid carbonic acid formation, which could lead to pipeline corrosion during its transportation. Since water is soluble in CO_2, when the two fluids come in contact water will evaporate in the CO_2 stream and will be transported following its advancing front (Figure 10). Due to this feature, water saturation may decrease under irreducible water saturation in the near wellbore area. Due to the decrease of the water liquid phase, salt will overcome the solubility limit and precipitate out of the solution, accumulating in the pore volume. This salt accumulation leads to a decrease in the near wellbore porosity and permeability which must be accurately modeled.

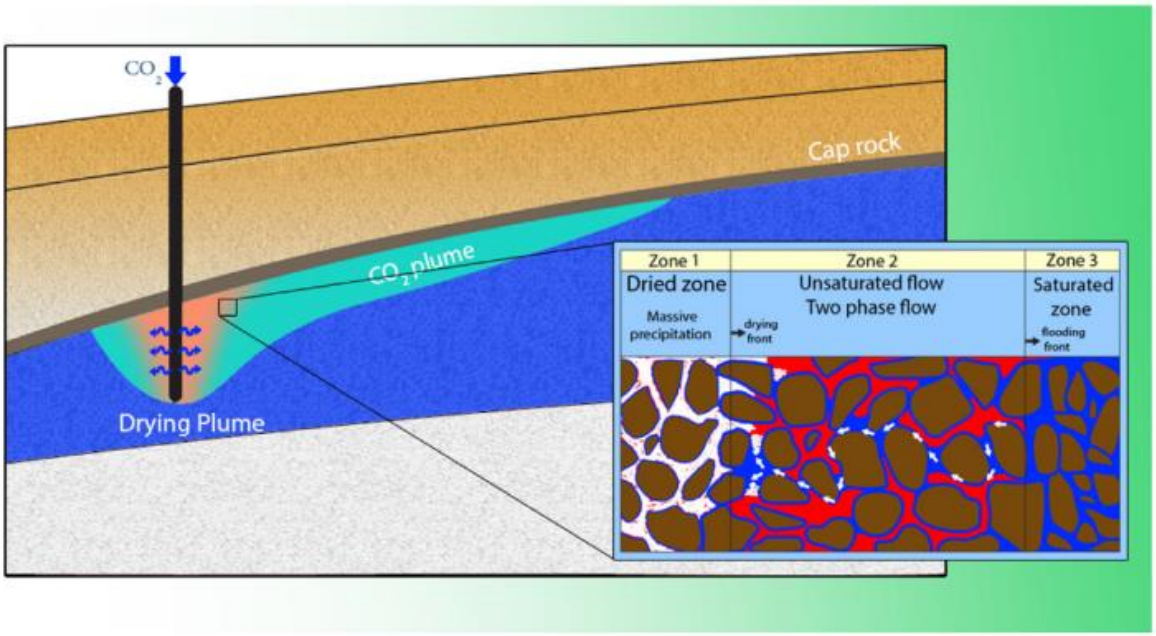

Figure 10 *Schematic representation of salt precipitation in the near wellbore area [30]*

Real CCS projects which consider MAS in saline aquifers are Decatur (Illinois) [34-35], Aquistor Southern Saskatchewan (Canada) [36-37] and Quest (Alberta) [38-39].

- Saline aquifer closures

Trapping mechanisms involved in CCS in saline aquifer closures are the same as those in open aquifers with few exceptions. First, hydrodynamic trapping does not occur but it is replaced by structural or stratigraphic trapping; second, the extent of all the other mechanisms (residual and geochemical) is much more limited (Figure 11). It is obvious that, due to the different dimensions considered, the storage capacity of a closure is much smaller if compared to open aquifers. This also makes maximum pressure a main constraint both to avoid fracturing during injection is planned and to assure caprock integrity at higher pressure values than the initial one. Final pressure may also re-activate existing sealing faults.

Like in open saline aquifers, saline aquifer closures are likely to have limited data availability but the area to be duly explored is limited. Oil and gas exploration dry holes can be used as a starting point for the characterization of a saline aquifer closure.

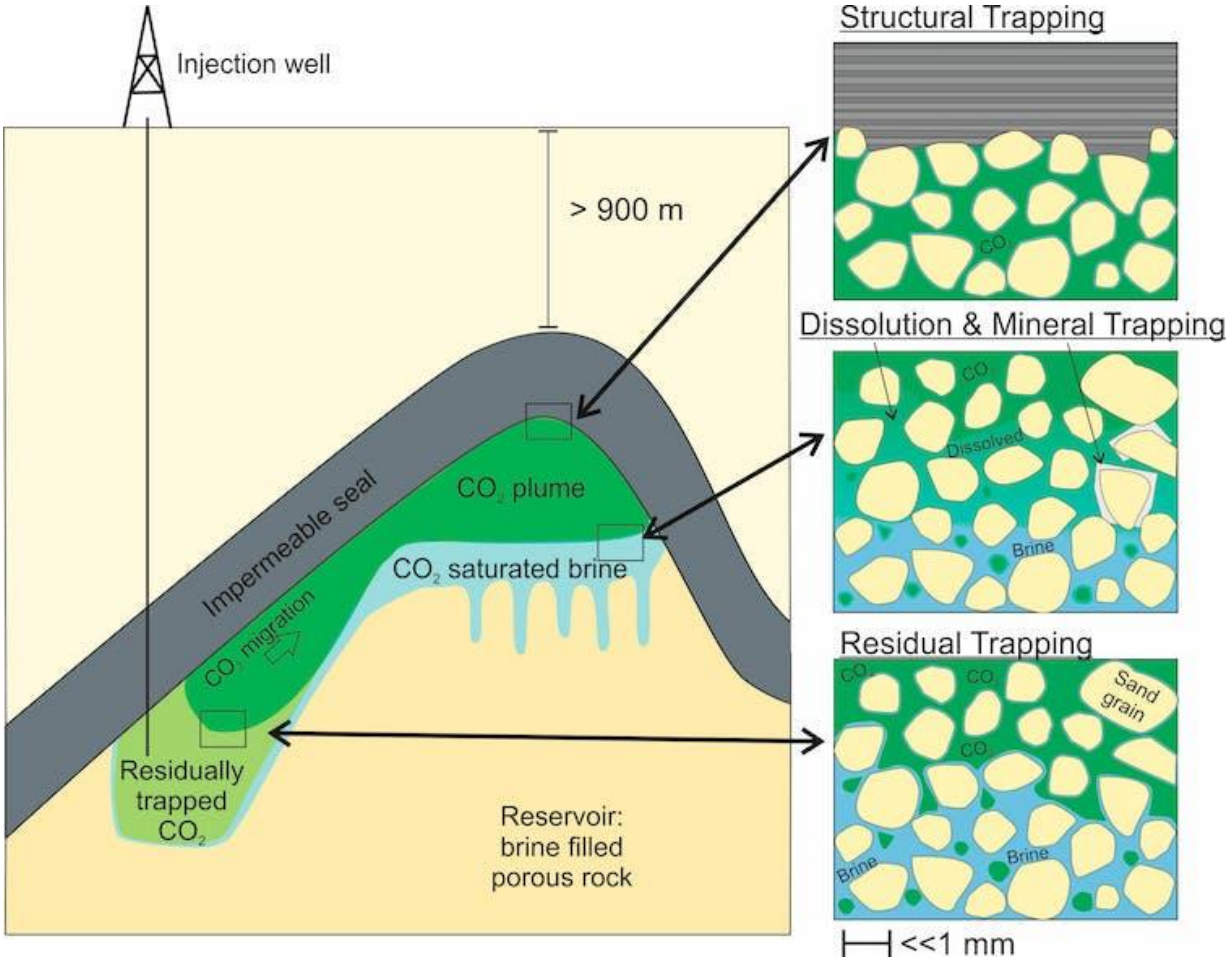

Figure 11 *Different trapping mechanisms in saline aquifer closure storage [40]*

- Depletion drive hydrocarbon reservoirs

Depleted reservoirs are feasible targets for CCS projects. CO_2 can be also injected in depleting reservoirs to perform EOR [41-44]. The main trapping mechanism on which these storage sites are based in a short time frame is structural/stratigraphic trapping (Figure 12). When injection is completed, some CO_2 may be residual trapped during its pathway but this quantity, compared with structural/stratigraphic trapped, is minor because hydrocarbons occupy part of the pore volume available for residual trapping. Geochemical trapping mechanisms are generally not considered for depleted reservoirs because the quantity of brine available, which is the main driver of these kind of mechanisms, is limited compared to aquifers.

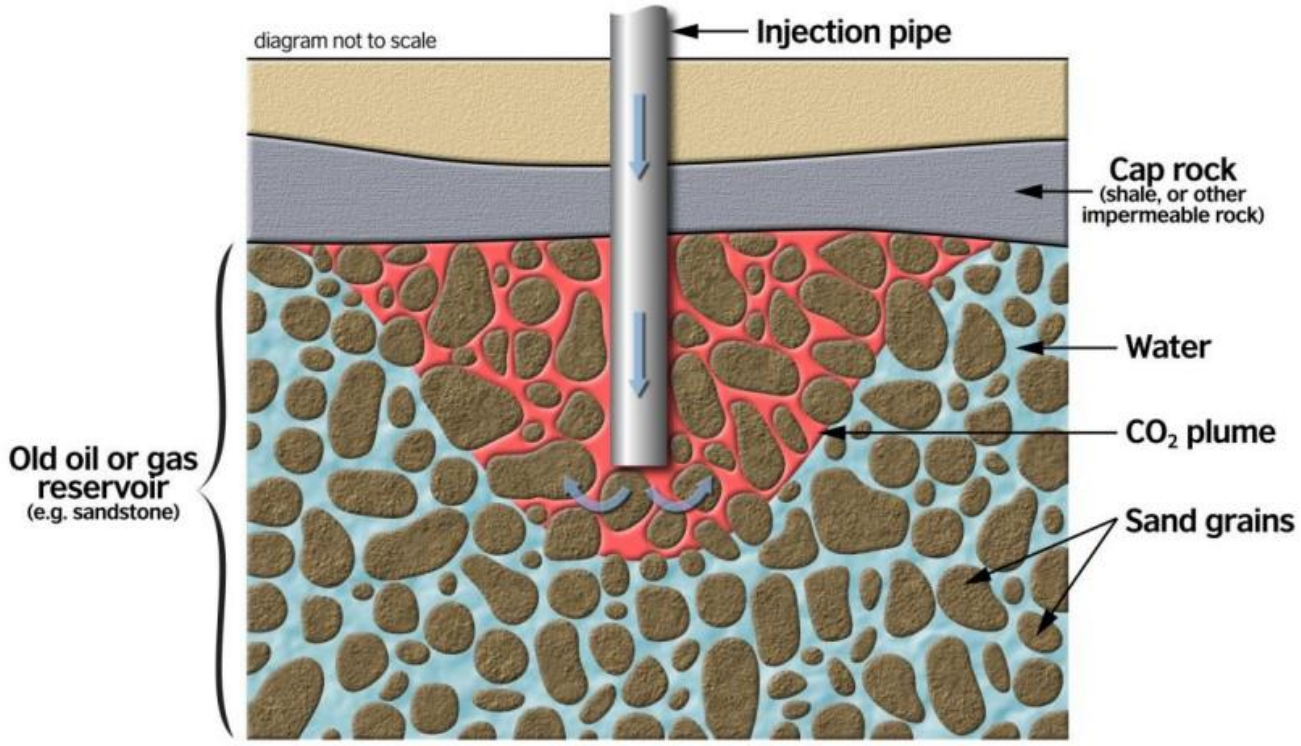

Figure 12 *Injection of carbon dioxide into depleted oil and gas reservoir [45]*

The main advantage of using depletion drive reservoirs relies on the fact that the target formation is generally already well known: static and dynamic datasets already exist. When depletion occurred many years before intended CO_2 storage, these datasets could be unreliable or outdated as depletion might have modified reservoir and caprock properties; in these cases new data must be acquired.

Since hydrocarbons were naturally trapped under the reservoir caprock, its integrity is reasonably proved also for CO_2 storage. However, further analysis must be performed to ensure the carbonic acid formed by injected CO_2 and the brine existing in reservoir as irreducible water saturation may attack and dissolve caprock minerals, potentially increasing caprock porosity and permeability. When production wells were drilled through the caprock, caprock integrity was compromised. Furthermore, if completions or cementations of abandoned wells were not done properly, wells integrity might not be guaranteed and CO_2 might leak to surface [18].

In depletion drive reservoirs there is no aquifer thus pressure increases only as a consequence of CO_2 injection. Even temporary overpressure issues might compromise the caprock integrity, thus geomechanics analysis are needed. To limit overpressure, the injection rate should be drastically reduced compromising the feasibility of the CCS project.

If supercritical CO_2 is injected at a much higher pressure than depleted reservoir pressure, its expansion may be accompanied by an adiabatic cooling defined as Joule-Thompson effect [46-47]. If this cooling is significant, residual formation water may freeze altering not only injectivity and formation permeability but also geomechanics of the rock, resulting in a higher probability of fracturing. If the injection point is too close to the sealing layer, caprock integrity may be compromised due to the fact that stresses may overcome tensile strength at low temperatures [48]. Joule-Thompson effect is minor

(cooling magnitude stays above few Celsius degrees) when the target formation is an aquifer, due to higher pressures that depleted reservoirs [49].

Just like when CO_2 is injected in aquifers, water evaporation in the near wellbore zone, which leads to salt precipitation, remains an issue that must be addressed even if its magnitude is minor [33].

Porthos (Nederlands) [50], Sleipner (Norway) [51] and In-Salah (Algeria) [52-54] are CCS projects using depleted gas reservoirs as target storage, while in Farnsworth field, Texas (USA) [55] and Weyburn, Saskatchewan (Canada) [56] CO2 injection was implemented as an EOR process to an oil field.

1.6 CCS numerical simulation

As previously discussed, the large variability in the targets for carbon dioxide storage add several complexities to perform evaluations before projects are effectively undertaken. The single contribution of each individual mechanism is also difficult to assess as CO_2 trapping largely depends not only on the fluid-rock mineral properties of the reservoir or aquifer under consideration but also on the CO_2 injection strategy; furthermore, each trapping mechanism is dependent on each other [23]. Numerical models can be used to predict the extent of each trapping mechanism under different conditions of interest [57] and to evaluate the feasibility of CO_2 storage projects. Ghanbari et al. [58] investigated key parameters affecting the solubility trapping mechanisms and the effect of convective flow patterns. Ukaegbu et al. [59] focused their study on the distribution of CO_2 between the aqueous and gaseous phases under several aquifer scenarios. Juanes et al. [60] demonstrated the importance of considering hysteresis effects in saline aquifer since it contributes to reduce CO_2 migration and accumulation along seal layers. Pruess et al. [61] investigated both mineral and solubility trapping mechanisms during CO_2 disposal in aquifer, analyzing porosity and permeability variation. Jobard et al. [62] carried out sensitivities analyses to study the contribution of solubility and mineral trapping mechanisms under different pressure and temperature conditions. Kumar and Bryan [63], Li et al. [64], Khudaida et al. [65] and Urych et al. [66] conducted simulation studies to investigate the plume behavior and CO_2 trapping under different injection strategies. Furthermore, different trapping mechanisms were also studied singularly: Arif et al. [67], Al-Khdheeawi et al. [68] and Ali et al. [69] focused on structural/stratigraphic and hydrodynamic trapping; Pentland et al. [70] deeply investigated how capillary forces contribute to residual trapping; Iglauer [71] studied solubility trapping and Golding et al. [72] and Al-Khdheeawi et al. [73] provided simulations on how geochemical reactions contribute to mineral trapping.
Thanks to these and many other studies, numerical simulators implemented modules specifically designed to simulate CO_2 injection and storage and able to account for all the features and issues related to CCS projects.

1.7 Objectives of the thesis

When modelling CO_2 storage, the effect of the trapping mechanisms is also controlled by simulation parameters such as grid discretization. Ideally, an accurate assessment of the different trapping mechanisms would require high resolution models in order to better describe the migration paths of the injected CO_2 in the subsurface. However, the discretization plays a key role in the simulation run time and thus on the feasibility of the study. In the first part of this thesis, the effects of grid discretization on bottom-hole pressure and carbon dioxide residual and solubility trapping are investigated on a synthetic case using CMG-GEM, an equation-of-state compositional, chemical and unconventional reservoir

simulator able to simulate coupled geochemical reactions, fluid flow, and CO_2 trapping mechanisms. In order to prove the consistency of these first results, the synthetic model was implemented using two other simulation software: ECLIPSE100 (by Schlumberger), a black-oil simulator which utilizes PVT data and fluid properties tables instead of equations of state [74], and Rubis (by Kappa) commonly used for well testing analysis. Eventually the results obtained from CMG-GEM were compared with the results obtained from the two other software in terms of bottom-hole pressure. Further investigations were made regarding gridding effects on different trapping mechanisms using CMG-GEM only.
Other model parameters that may have significant impact on the simulation results are the geochemical initial conditions. To evaluate them, several geochemical scenarios were developed and sensitivities analyses were performed and discussed in the second part of this thesis and compared to what can be found in literature.

2. Model description

A simplified 3D numerical model (Figure 13) representing a portion of a deep saline aquifer was set up using CMG-GEM. The model dimensions are 1350x1350x31 m^3; a single injector well is located in the middle. The depth of the aquifer top was set at 1500 m.
The aquifer thickness is 20 m and the thickness of the overlying caprock is 10 m. A monitor layer above the caprock was also defined to monitor any possible leak of the injected CO2 through the caprock. The monitor layer is 1 m thick.

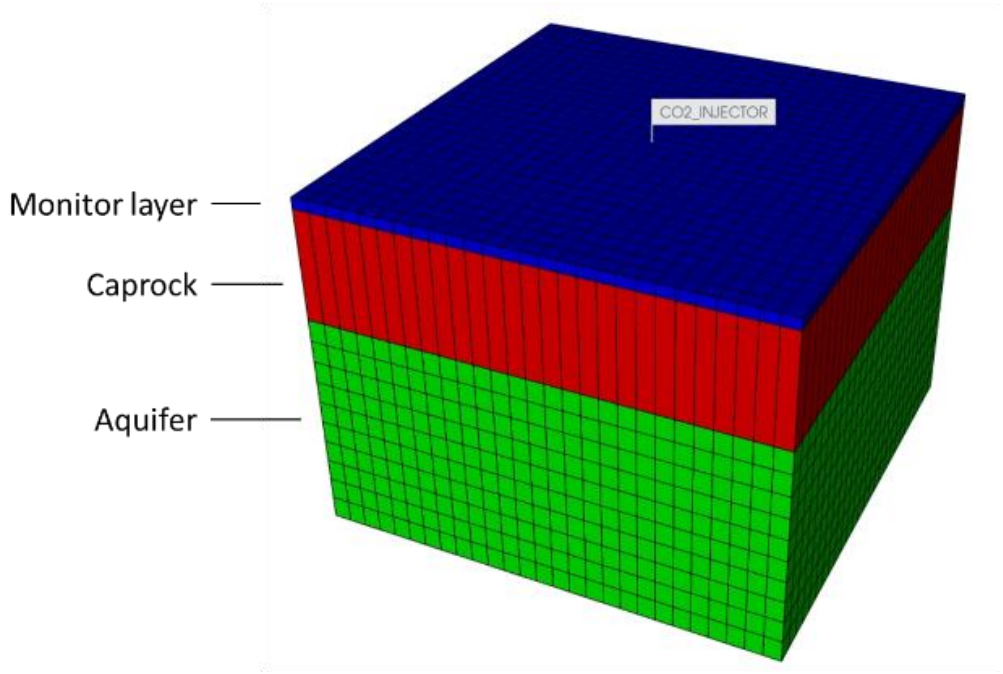

Figure 13 *3D synthetic model used in GEM showing the three zones: aquifer, caprock and monitor layer, and the uniform discretization*

2.1 Gridding options

The simulations were performed with the aim to assess the impact of discretization on CO2 fluid-flow behavior and trapped quantities according to the different mechanisms. Initially, the bottom-hole pressure during CO2 injection was monitored. Under the assumption that multi-phase fluid-flow prevails during CO2 early injection the commercial black-oil simulator Eclipse 100 (Schlumberger) was also used to benchmark the obtained results, while the commercial black-oil simulator Rubis (Kappa) was used to assess more gridding options. Then, the impact of the model discretization on the CO2 trapped by the different mechanisms was assessed by simulating CO2 injection and a subsequent monitoring period using GEM.
The petrophysical characteristics and the rock-fluid interaction properties were the same for all the models. Conversely, as described further on, the boundary conditions and the PVT properties had to be set differently in the used software due to their different capabilities.

The effect of grid discretization on the simulated bottom-hole pressure and trapping mechanisms was evaluated using GEM by considering four grids with different discretization (G1, G2, G3, G4). The vertical layering of the aquifer was kept constant, with each layer having a thickness of 2 m. In grids G1, G2 and G3 the block areal dimensions are constant in the area close to the well. Conversely, G4 was built

using different block dimensions according to their distance from the well: in the area surrounding the well blocks have a 2x2 m areal dimension, which progressively increases moving towards the model boundaries up to 145x145 m. The grid parameters for the 4 investigated cases are reported in Table 1 and shown in Figure 14.

Table 1 *Gridding parameters*

	G1	G2	G3	G4
Top grid depth	1500 m			
Aquifer dimensions	1350x1350x20 m^3			
N° of blocks	7290 (27x27x10)			
Block dimensions (i,j,k)	50x50x2 m^3	25x25x2 m^3	15x15x2 m^3	2x2x2 ÷ 145x145x2 m^3

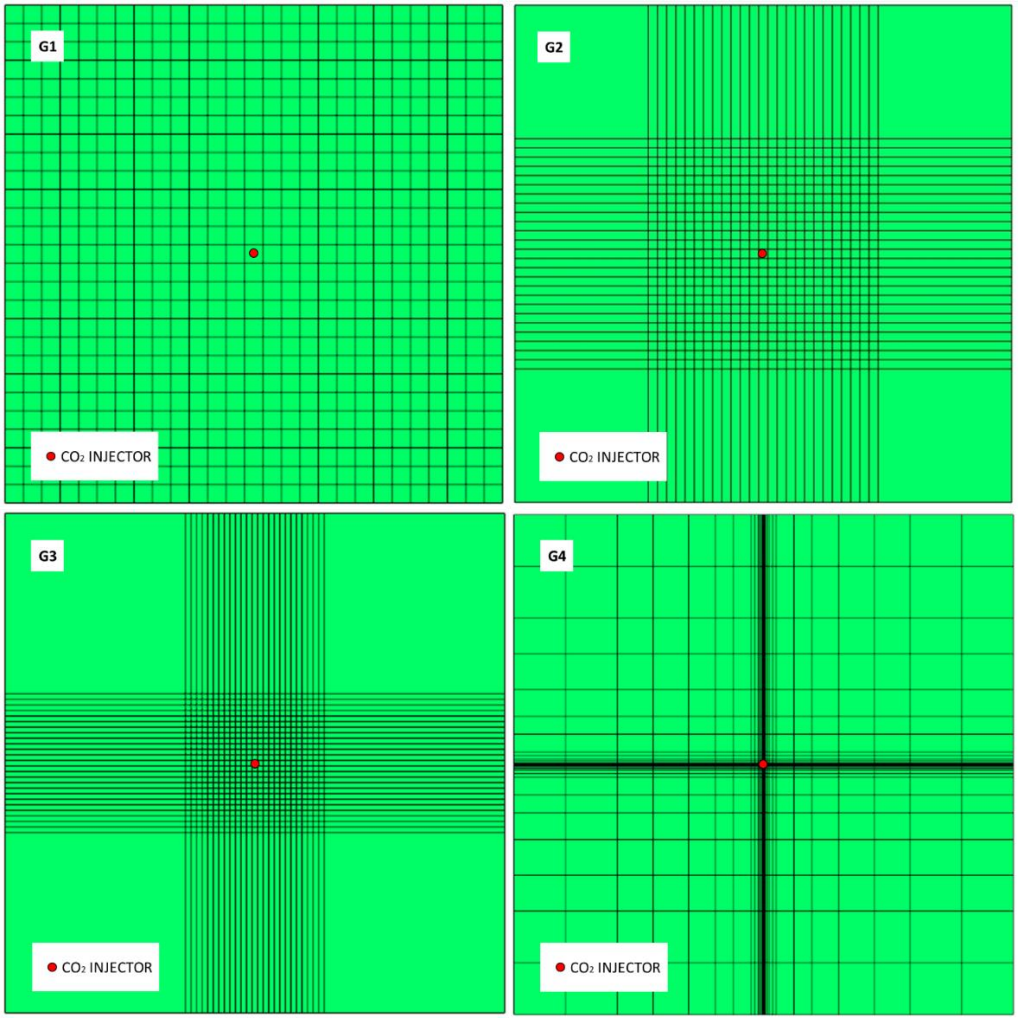

Figure 14 *Grid discretization used in GEM*

The bottom of the aquifer was set as a no-flow boundary. An analytical infinite Carter-Tracy aquifer was adopted as a lateral boundary condition allowing water to exit and enter the model domain. Because the

water is the only component allowed to flow through the boundary, a sufficient distance between the CO_2 plume and the interface with the analytical aquifer was guaranteed so as to prevent the accumulation of CO_2 in the external blocks of the model. The initial conditions applied to the synthetic aquifer are given in Table 2.

Table 2 *Initial conditions of the aquifer*

Datum depth	1500 *m*
Initial aquifer temperature	50 °C
Initial aquifer pressure	150 bars

The same grid options used in GEM (Table 1) as well as the same aquifer initial conditions were also used in Eclipse 100 (the grids were named E1, E2, E3 and E4)

A different approach was used for Rubis as the software does not allow the definition of an analytical aquifer. In order to reproduce an infinite aquifer, the model dimensions were increased to 300x300 km. The grid geometry is hexagonal with a refinement in the near-wellbore area (Figure 15). The grid refinement area developing around the well is controlled by the progressive ratio (PR): by decreasing the PR value the refinement increases. This grid refinement approach is particularly effective to simulate the pressure history during CO_2 injection. Four different grids (named R1, R2, R3 and R4), were generated adopting four different progressive ratios (Table 3 and Figure 15). The depth of the aquifer top as well as the initial conditions of the aquifer used in Rubis are the same as those used in GEM (Tables 1 and 2).

Table 3 *Grid parameters in Rubis*

GRID	PR	Number of angular divisions	Number of horizontal layers	Total number of blocks
R1	4.0	12	10	6510
R2	2.5	12	10	6930
R3	1.7	12	10	7890
R4	1.4	12	10	9090

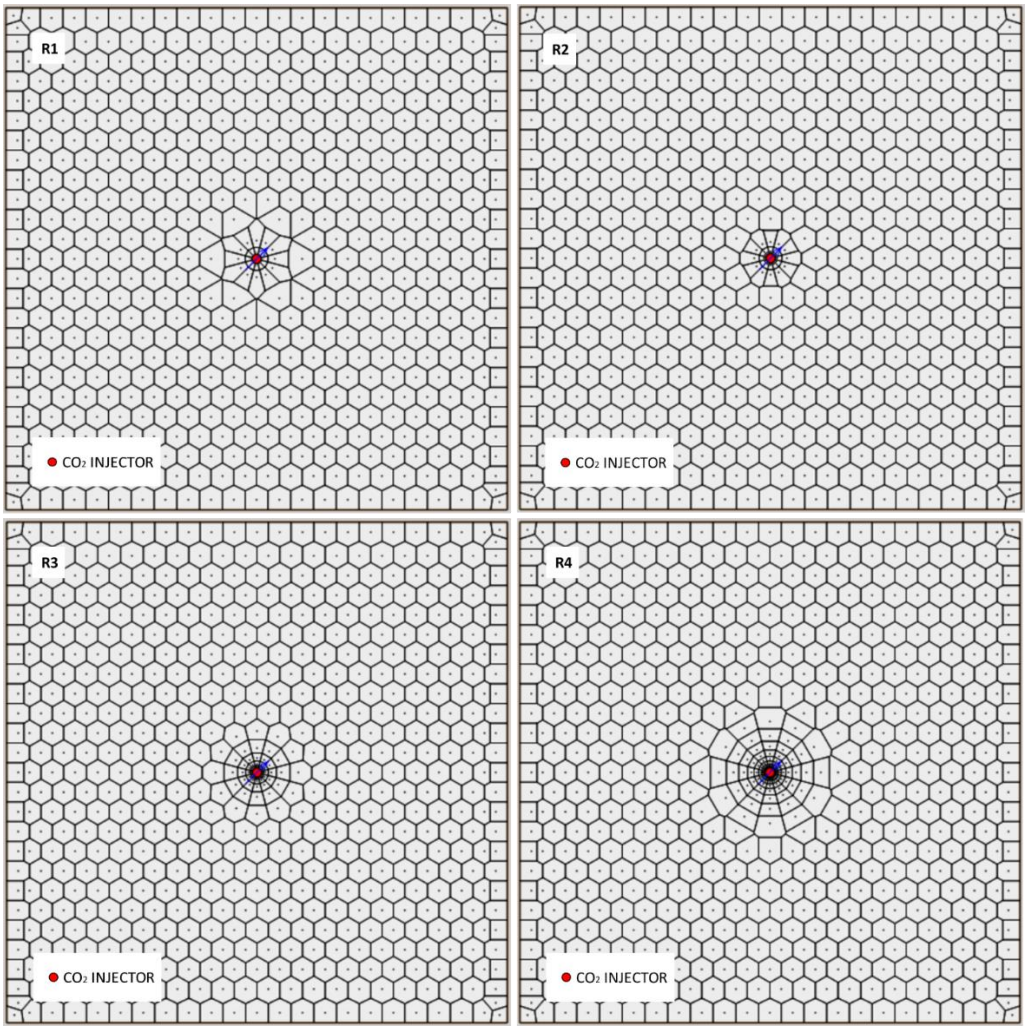

Figure 15 *Grid discretization used in Rubis*

2.2 Rock and fluid properties

The rock and fluid properties used for characterizing the synthetic model are typical values for a 1500-deep aquifer and they are summarized in Table 4 [75-77].

Table 4 *Rock and fluid properties*

Aquifer porosity	0.2
Aquifer permeability	200 mD
Anisotropy ratio	1.0
Rock compressibility	$4.5 \cdot 10^{-5}$ bar^{-1}
Water compressibility	$4.35 \cdot 10^{-5}$ bar^{-1}
Reference pressure for compressibility	150 bar
Water density (at standard conditions)	1020 kg/m^3
Water salinity (NaCl)	10000 ppm

The permeability of the caprock was set equal to 10^{-7} mD [18]. The relative permeability curves were calculated according to Corey-Brooks method [78] using the following exponents and end points from the literature: $N_w = 5$ [79], $N_{CO2} = 2$ [80], $S_{wi} = 0.307$, $S_{gc} = 0.106$ and $S_{ghys} = 0.4$ [81]. The capillary pressure curves were also taken from experimental data reported in the literature [82]. The relative permeability and capillary pressure curves are shown respectively in Figure 16 and Figure 17.

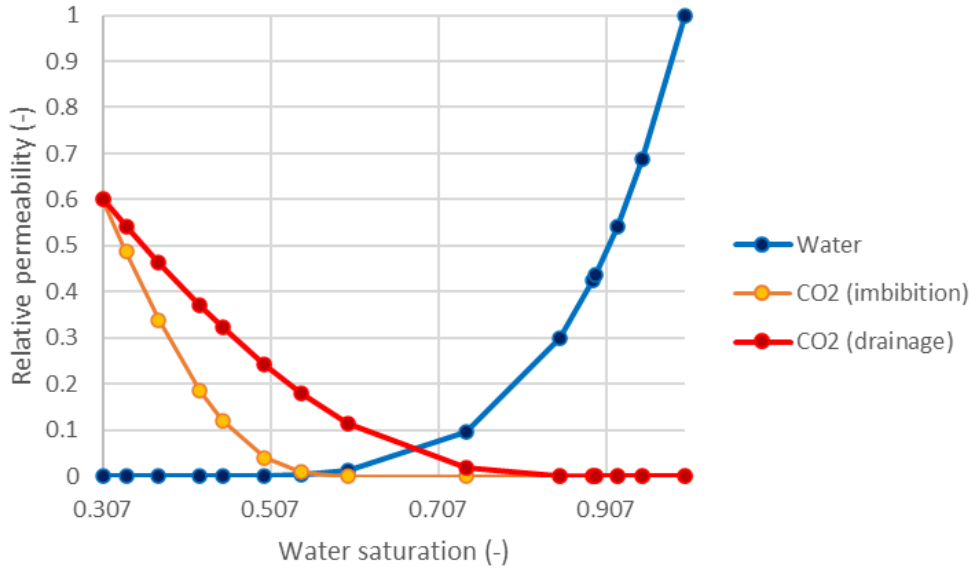

Figure 16 *Relative permeability curves*

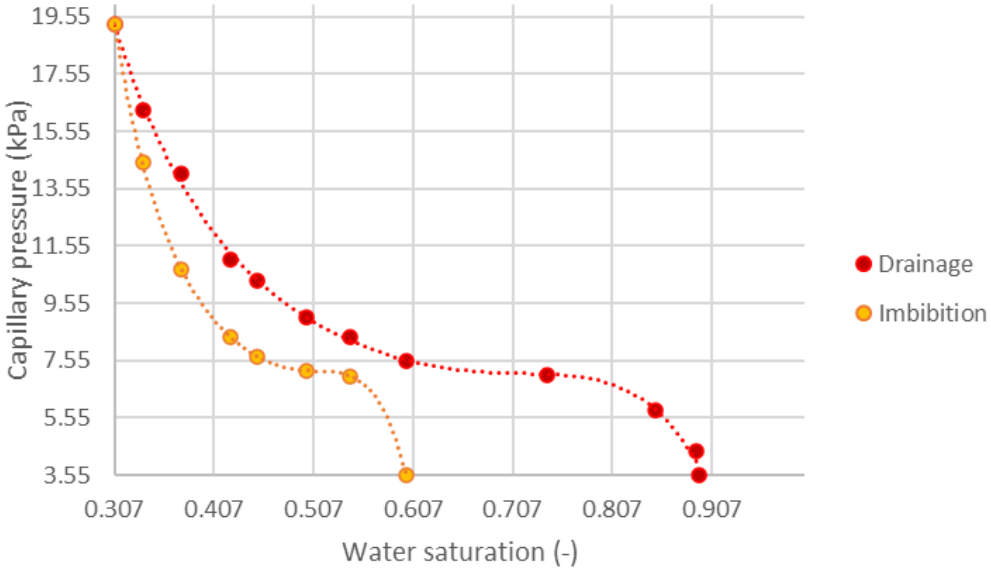

Figure 17 *Capillary pressure curves*

2.3 Geochemistry

In GEM the CO_2 PVT properties were calculated by the software based on the CO_2 critical properties ($T_c = 304.2\ K, P_c = 72.8\ atm$) and acentric factor ($\omega = 0.225$) [83-84]; the Peng-Robinson [85] equation of state was used. The same rock-fluid properties as well as the PVT model used in GEM were also adopted in Eclipse 100. In Rubis, the CO_2 PVT properties were taken from the software internal database for pure CO_2.

Solubility is applied in GEM by the use of Harvey's correlation for CO_2 Henry's constant [86], but with a modified form of the molar volume function for calculating Henry's constant at high pressure. This correlation is applicable up to 150° C and 1100 bar. The use of this option makes the Henry's constant a function of pressure, temperature and salinity.

Aqueous reactions (reactions (9) to (16)) as well as mineral reactions (reactions (17) to (27)) considered in the simulation are taken from Wolery's database [87] and the relative parameters are summarized in Table 5. To perform all the simulations, the B-DOT reactivity model was used because it is the preferred method for ionic coefficients when the solution is non-ideal [88].

$$Al(OH)_4^- + 4H^+ \leftrightarrow Al^{3+} + H_2O$$

(9) Dissociation aluminate - W23

$$CO_2 + H_2O \leftrightarrow H^+ + HCO_3^-$$

(10) Dissociation of carbon dioxide in bicarbonate - W82

$$CO_3^{2-} + H^+ \leftrightarrow HCO_3^-$$

(11) Dissociation of bicarbonate in carbonate ions - W83

$$CaCl^+ \leftrightarrow Ca^{2+} + Cl^-$$

(12) Dissociation of calcium chloride - W89

$$CaHCO_3^+ \leftrightarrow HCO_3^- + Ca^{2+}$$

(13) Dissociation of calcium bicarbonate – W93

$$MgCl^+ \leftrightarrow Mg^{2+} + Cl^-$$

(14) Dissociation of magnesium chloride – W256

$$MgHCO_3^+ \leftrightarrow HCO_3^- + Mg^{2+}$$

(15) Dissociation of magnesium bicarbonate – W261

$$OH^- + H^+ \leftrightarrow H_2O$$

(16) Dissociation of water in hydroxide and hydrogen ions – W355

$$CaAl_2(SiO_4)_2 + 8H^+ \leftrightarrow 2Al^{3+} + 4H_2O + Ca^{2+} + 2SiO_2$$

(17) Precipitation/dissolution of anorthite – W31

$$CaCO_3 + H^+ \leftrightarrow Ca^{2+} + HCO_3^-$$

(18) Precipitation/dissolution of calcite – W113

$$Fe_2Al_2SiO_5(OH)_4 + 10H^+ \leftrightarrow 2Al^{3+} + 2Fe^{2+} + 7H_2O + SiO_2$$

(19) Precipitation/dissolution of chamosite-7A (chlorite) – W122

$$CaMg(CO_3)_2 + 2H^+ \leftrightarrow Ca^{2+} + 2HCO_3^- + Mg^{2+}$$

(20) Precipitation/dissolution of dolomite – W195

$$NaCl \leftrightarrow Na^+ + Cl^-$$

(21) Precipitation/dissolution of halite – W257

$$K_{0.6}Mg_{0.25}Al_{2.3}Si_{3.5}O_{10}(OH)_2 + 8H^+ \leftrightarrow 2.3Al^{3+} + 5H_2O + 0.6K^+ + 0.25Mg^{2+} + 3.5SiO_2$$

(22) Precipitation/dissolution of illite – W274

$$KAlSi_3O_8 + 4H^+ \leftrightarrow Al^{3+} + 2H_2O + K^+ + 3SiO_2$$

(23) Precipitation/dissolution of K-feldspar – W279

$$Al_2Si_2O_5(OH)_4 + 6H^+ \leftrightarrow 2Al^{3+} + 5H_2O + 2SiO_2$$

(24) Precipitation/dissolution of kaolinite – W293

$$FeS_2 + H_2O \leftrightarrow Fe^{2+} + 0.25H^+ + 1.75HS^- + 0.25SO_4^{2-}$$

(25) Precipitation/dissolution of pyrite – W445

$$SiO_2 \leftrightarrow SiO_{2(aq)}$$

(26) Precipitation/dissolution of quartz – W449

$$FeCO_3 + H^+ \leftrightarrow Fe^{2+} + HCO_3^-$$

(27) Precipitation/dissolution of siderite – W488

Table 5 *Geochemistry reactions parameters (a0, a1, a2, a3 and a4 define the chemical equilibrium constant through the equation* $log_{10}(K_{eq}) = a0 + a1 \cdot T + a2 \cdot T^2 + a3 \cdot T^3 + a4 \cdot T^4$*; area0 is the initial reactive surface area; e_act is the activation energy; k0_ref is the logarithm of k0 and t_ref is the reference temperature for k0_ref) [87].*
**[89-90]*

Reaction	a0	a1	a2	a3	a4	area0 (m^2/m^3)	e_act (J/mol)	k0_ref (mol/m^2s)	t_ref (°C)
W23 (aluminate)	25.462	-0.16	0.001	-4e-6	6e-9	-	-	-	-
W82 (bicarbonate)	-6.549	0.009	-1e-4	3e-7	-4e-10	-	-	-	-
W83 (carbonate ions)	10.608	-0.013	1e-4	-3e-7	3e-10	-	-	-	-
W89 (Ca chloride)	-0.967	0.013	-1e-4	4e-7	-7e-10	-	-	-	-
W93 (Ca bicarbonate)	-1.187	0.002	-1e-4	9e-7	-2e-9	-	-	-	-
W256 (Mg chloride)	-0.353	0.011	-1e-4	4e-7	-7e-10	-	-	-	-
W261 (Mg bicarbonate)	-0.981	-3e-4	-4e-5	2e-7	-5e-10	-	-	-	-
W355 (water ions)	14.298	-0.042	2e-4	-6e-7	8e-10	-	-	-	-
W31 (anorthite)	31.746	-0.201	6e-4	-9e-7	9e-11	2760.29	16600	-3.5	25
W113 (calcite)	2.069	-0.014	-6e-6	1e-7	-4e-10	2709.95	14400	-0.3	25
W122 (chlorite)	39.049	-0.244	8e-4	-1e-6	4e-10	290.73*	41870	-8.8	25
W195 (dolomite)	3.394	-0.036	1e-5	2e-7	-8e-10	2864.96	36100	-3.19	25
W257 (halite)	1.501	0.005	-6e-5	2e-7	-4e-10	2163.35	7400	-0.21	25
W274 (illite)	12.435	-0.112	3e-4	-8e-8	-8e-10	2763.07	23600	-10.9788	25
W279 (K-feldspar)	0.461	-0.015	-4e-5	4e-7	-9e-10	355.47*	41870	-8.8	25
W293 (kaolinite)	9.73	-0.099	3e-4	-3e-7	-3e-10	2594.05	65900	-11.3098	25
W445 (pyrite)	-26.521	0.082	-4e-4	1e-6	-1e-9	5011.15	90900	-8.19	25
W449 (quartz)	-4.497	0.022	-1e-4	3e-7	-4e-10	2650	90900	-13.4	25
W488 (siderite)	0.254	-0.019	9e-6	1e-7	-4e-10	4046.67	36100	-3.19	25

To investigate the effect of considering different geochemical properties on the simulated trapping mechanisms, a total of 12 geochemical scenarios (Table 8) were developed and implemented in GEM. The scenarios were built by combining the following real datasets, kindly made available by a large gas industry:

- 4 brine chemistry datasets (Table 6)
- 3 mineralogy datasets (Table 7).

To understand the result discussion in section 4.4, it should be noted that the simulations were made by coupling water chemistry and rock mineralogy as reported in Table 8.

Table 6 *Brine chemistry dataset implemented in geochemistry scenarios used in GEM*
**CC = free cations concentration (ppm)*

Brine chemistry dataset	A1	A2	A3	A4
Initial pH	5.43	5.53	5.74	5.96
Initial aqueous concentration (ppm)				
Ca^{2+}	3174	4500	42000	8800
Mg^{2+}	1499	2104	780	1320
K^{+}	269	364	1230	387
Na^{+}	15510	21900	13271	21628
SO_4^{2-}	131	129	50	50
Al^{3+}	1	1	1	1
Fe^{2+}	32	32	214	120
SiO_2	172	172	172	172
HS^{-}	1	1	1	1
Cl^{-}	59846	60509	110668	48799
Log(CC)	4.31	4.46	4.76	4.51

Table 7 *Mineralogy dataset implemented in geochemistry scenarios used in GEM*

Mineralogy dataset	M1		M2		M3	
Initial volume fraction	**Aquifer**	**Caprock and Monitoring**	**Aquifer**	**Caprock and Monitoring**	**Aquifer**	**Caprock and Monitoring**
Calcite	21.6%	30%	34.5%	30%	17.9%	30%
Dolomite	40.4%	18.2%	24.5%	18.2%	21.9%	18.2%
Illite	8.2%	15.4%	6.1%	15.4%	16.4%	15.4%
K-feldspar	7.6%	7%	5.9%	7%	5.4%	7%
Kaolinite	2.1%	2.8%	2.4%	2.8%	1%	2.8%
Pyrite	0.1%	0.3%	0.3%	0.3%	0%	0.3%
Anorthite	4.2%	5.5%	4.9%	5.5%	5.1%	5.5%
Halite	0%	0.1%	0.4%	0.1%	0%	0.1%
Quartz	13.3%	18.1%	19%	18.1%	30.8%	18.1%
Chamosite-7A (chlorite)	2.5%	2.1%	2%	2.1%	1.2%	2.1%
Siderite	0%	0.5%	0%	0.5%	0.3%	0.5%

Table 8 *Geochemistry scenarios used in GEM*

Geochemical scenario	Brine chemistry dataset	Rock mineralogy dataset
GC1	A1	M1
GC2	A1	M2
GC3	A1	M3
GC4	A2	M1
GC5	A2	M2
GC6	A2	M3
GC7	A3	M1
GC8	A3	M2
GC9	A3	M3
GC10	A4	M1
GC11	A4	M2
GC12	A4	M3

The option of water vaporization due to CO_2 injection was activated and modeled through the introduction of a cut-off of the aqueous phase saturation, set at 0.1: below the cut-off all the geochemical reactions stop.

2.4 Injection strategy

In every simulation, the injector well was placed at the center of the model and its perforations were open in the 1510-1518 m depth interval. The well radius is equal to 0.0762 m. The rate of injected CO_2 was constant and equal to 200,000 sm^3/day, which is equivalent to a mass rate of 0.136 Mt/y. The duration of the injection is 120 days so that the CO_2 plume does not reach the model boundary over the entire simulation period (Figure 18) when grid discretization was studied. This same simulation strategy was adopted in Eclipse 100 and in Rubis.

2.5 Simulation parameters

Since simulation results are sensitive to numerical parameters used to perform the simulation itself, the following ones were adopted and used for the entire study in GEM:

- Maximum timestep size - DTMAX = 75 days
- Minimum timestep size - DTMIN = 1e-6 days
- Typical change of pressure over a timestep – NORM PRESS = 1000 kPa
- Typical change of saturation over a timestep – NORM SATUR = 0.01
- Typical change of global composition over a timestep – NORM GMOLAR = 0.005

- Typical change of aqueous component over a timestep – NORM AQUEOUS = 0.3
- Maximum change of pressure over a timestep – MAXCHANGE PRESS = 20000 kPa
- Maximum change of saturation over a timestep – MAXCHANGE SATUR = 0.8
- Maximum change of global composition over a timestep – MAXCHANGE GMOLAR = 0.8
- Convergence tolerance for pressure – CONVERGE PRESS = 1e-4 kPa
- Convergence tolerance for hydrocarbon molar density – CONVERGE HC = 1e-5
- Convergence tolerance for water molar density – CONVERGE WATER = 1e-5
- Convergence tolerance for any equation – CONVERGE MAXRES = 1e-4
- Linear solver precision – PRECC = 1e-6
- Linear solver iterations – ITERMAX = 200
- Linear solver orthogonalizations – NORTH = 200

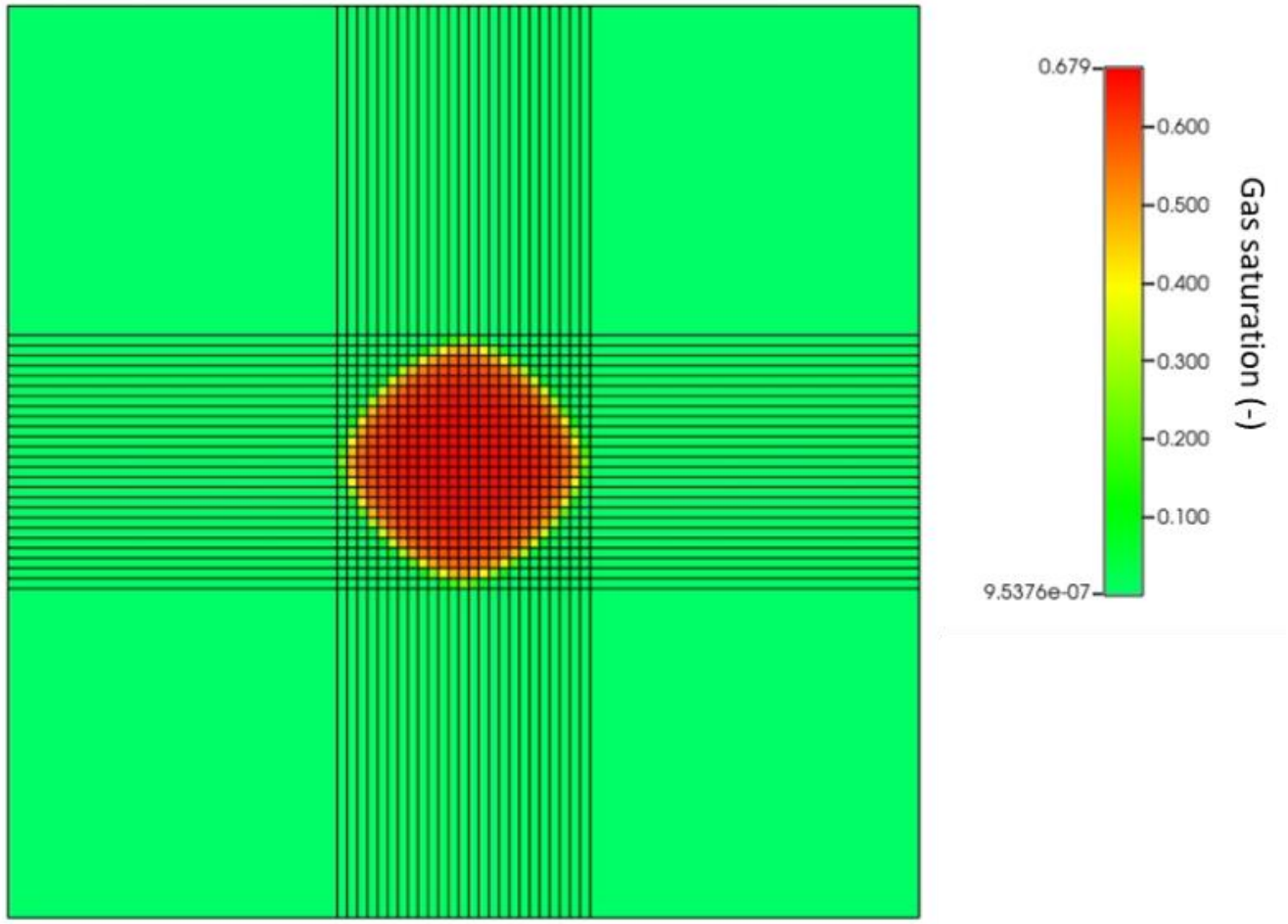

Figure 18 *CO_2 saturation at the end of injection in grid G3 (top layer of the aquifer)*

3. Methodology

The study of the effect of model gridding was carried out through the analysis of the simulation results obtained using the different grids described in section 2.1.

The first step focused on the impact of the discretization on the well bottom-hole pressure profiles through the analysis of the simulated results using GEM and also Eclipse 100 taken as a benchmark, based on the assumption that multiphase fluid-flow dominates during the very first stage of injection thus the compositional capabilities would have a limited impact on the wellbore pressure trend. Rubis was also used due to the possibility of defining very refined grids in the near well-bore area.

In a second step, three different injection history scenarios were assigned and the induced well bottom-hole pressure profiles were analyzed.

Then, the impact of discretization on residual and solubility trapping was studied by simulating 100, 200 and 500 years of CO_2 injection, respectively. In these cases, the rate of CO_2 injection was reduced to 10,000 sm^3/day (the injection period was kept equal to 120 days) in order to limit the plume of CO_2, both in free-phase and in solution, in the near-wellbore area where the grid was refined with respect to the base case scenario with uniform grid blocks and thus the gridding effects would potentially have a larger impact on the results. Mineral trapping was not considered in this first part of the study.

Regarding the study on different geochemistry, 12 different simulations were performed only in GEM using grid G1 and adopting different geochemical scenarios as discussed in section 2.3. The injection rate was ramped-up through 8 isochronal steps to 200,000 sm^3/day in 120 days (ramp-up injection scenario 3 defined in section 4.2) and then kept constant at that value for a total duration of injection of 1 year. In this way, the total mass of injected CO_2 is equal to 0.116 Mt. For this part of the study, simulations results were monitored after 200 and 1000 years.

The different scenarios are presented in Figure 19.

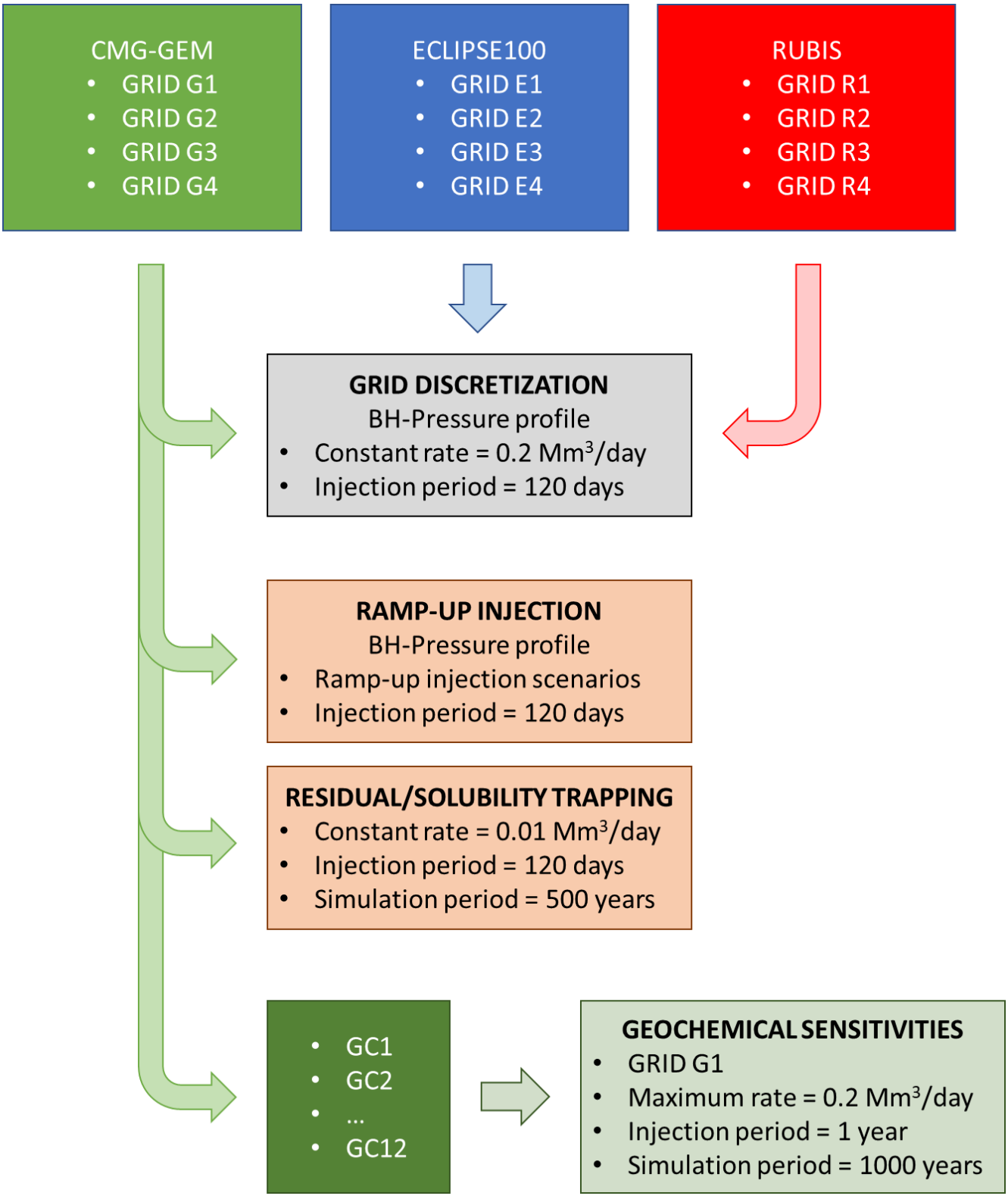

Figure 19 *Methodology*

4. Results

4.1 Grid discretization

The results of the simulations performed with GEM showed that when injection starts, the well bottom-hole pressure reaches a peak, then pressure progressively decreases until stabilizing (Figure 20). The value of this peak and the time to reach it are proportional to the dimension of the blocks (Table 9). The pressure peak ranges from 113% (G4) to 125% (G1) of the initial aquifer pressure; at the end of injection, the bottom-hole pressure reaches values ranging between 106.2% (G4) and 107.5% (G1).

Figures 21 and 22 respectively show the pressure distribution and how the CO_2 spreads laterally in the aquifer according to different gridding options.

The same pressure trends observed with GEM were confirmed by the Eclipse100 simulation results, even if the values of the overpressure peaks are different (Table 9 and Figure 23). Furthermore, also the reservoir pressure reached at the end of injection, ranging from 104.6% (E4) to 108.7% (E1), showed significant dependency on gridding.

When Rubis was used for the simulation of the same scenarios, the bottom-hole pressure peaks were much lower with respect to the ones observed in GEM and Eclipse 100 simulations as well as the time needed to reach the peak values (Figure 24). By increasing the near-wellbore grid refinement through the PR parameter the bottom-hole pressure peak decreases from 110.4% (grid R1, PR = 4.0) to 108.5% (grid R4, PR = 1.4) of the initial aquifer pressure. No significant effects on the bottom-hole pressure at the end of CO_2 injection is detected for the four grids.

In summary, all the sensitivities showed that the grid block dimensions always have a significant impact on the simulated overpressure during injection, and in most cases the maximum bottom-hole pressure largely exceeds the final overpressure value. To further confirm these results, it can be observed that the simulations performed with Rubis, which allowed the adoption of a very refined grid around the wellbore, are those providing the lower values of the local pressure increase at the wellbore.

Even though no CO_2 above the caprock was detected due to leakage induced by overpressure conditions, it should be noted that the effects of the caprock threshold pressure and mostly the geomechanics of the system were not simulated. Should a more comprehensive assessment be performed, the simulated peak pressure values would likely not be acceptable. However, these pressure peaks at the wellbore are not due to physical phenomena but are only due to modeling issues thus they are not representative of the response of the real system. Furthermore, while the results on the pressure trend induced during injection were expected, the question is to which extent the model discretization can affect the quantity of CO_2 trapped in the aquifer by the different trapping mechanisms.

Table 9 *Grid discretization effects on well bottom-hole pressure profiles*

GRID	Bottom-hole pressure peak (bar)	Peak overpressure (bar)	Time needed to reach the pressure peak (days)	Final bottom-hole pressure (bar)
G1	188.4	37.3	2.08	162.5
G2	184.6	33.5	0.52	161.1
G3	182.3	31.2	0.19	160.8
G4	170.6	19.5	<0.01	160.5
E1	210.6	59.5	2.3	164.3
E2	201.7	50.6	0.6	160.8
E3	195.8	44.7	0.2	159.3
E4	188.5	37.4	<0.01	158.0
R1	166.8	15.7	<0.01	160.7
R2	165.2	14.1	<0.01	160.9
R3	164.5	13.4	<0.01	160.8
R4	163.9	12.8	<0.01	160.8

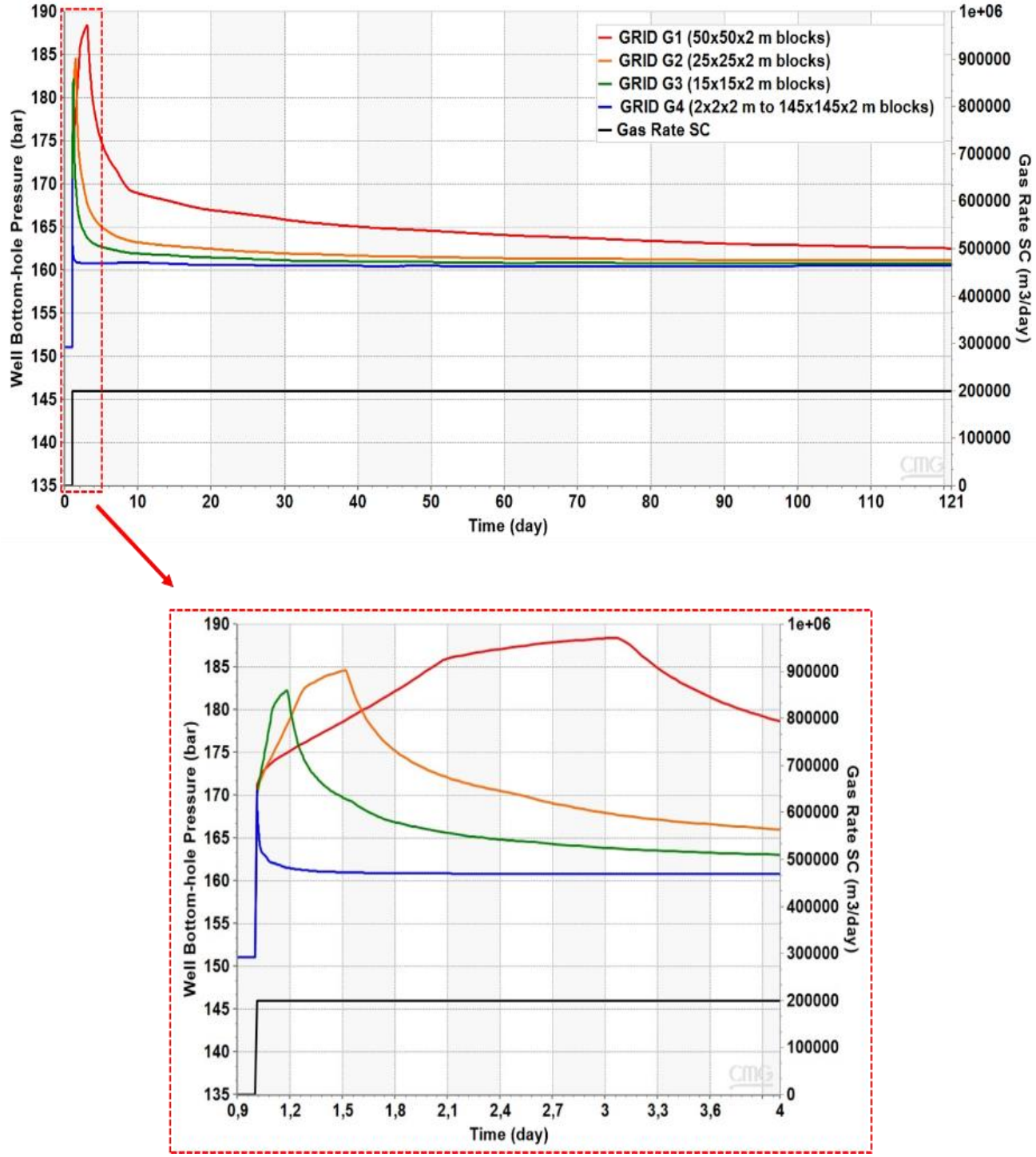

Figure 20 *Well bottom-hole pressure profiles for grids G1, G2, G3 and G4*

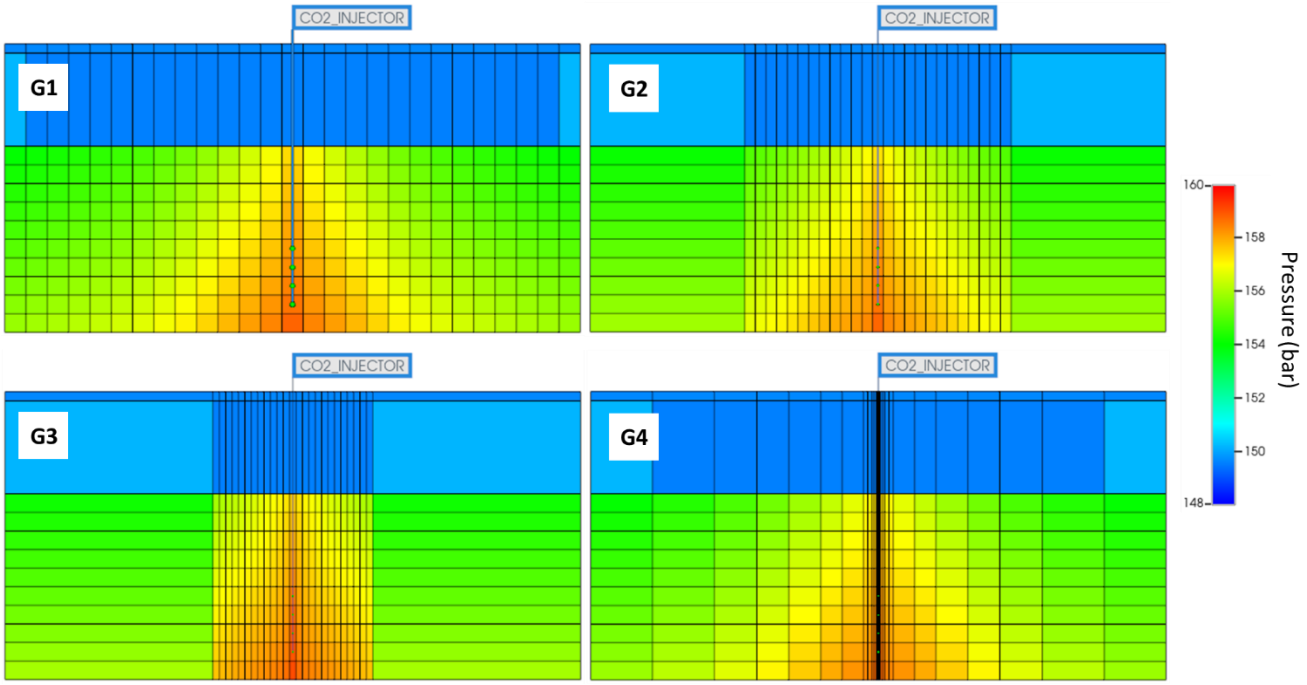

Figure 21 *Pressure distribution after injection for different gridding in GEM (IK 2D view)*

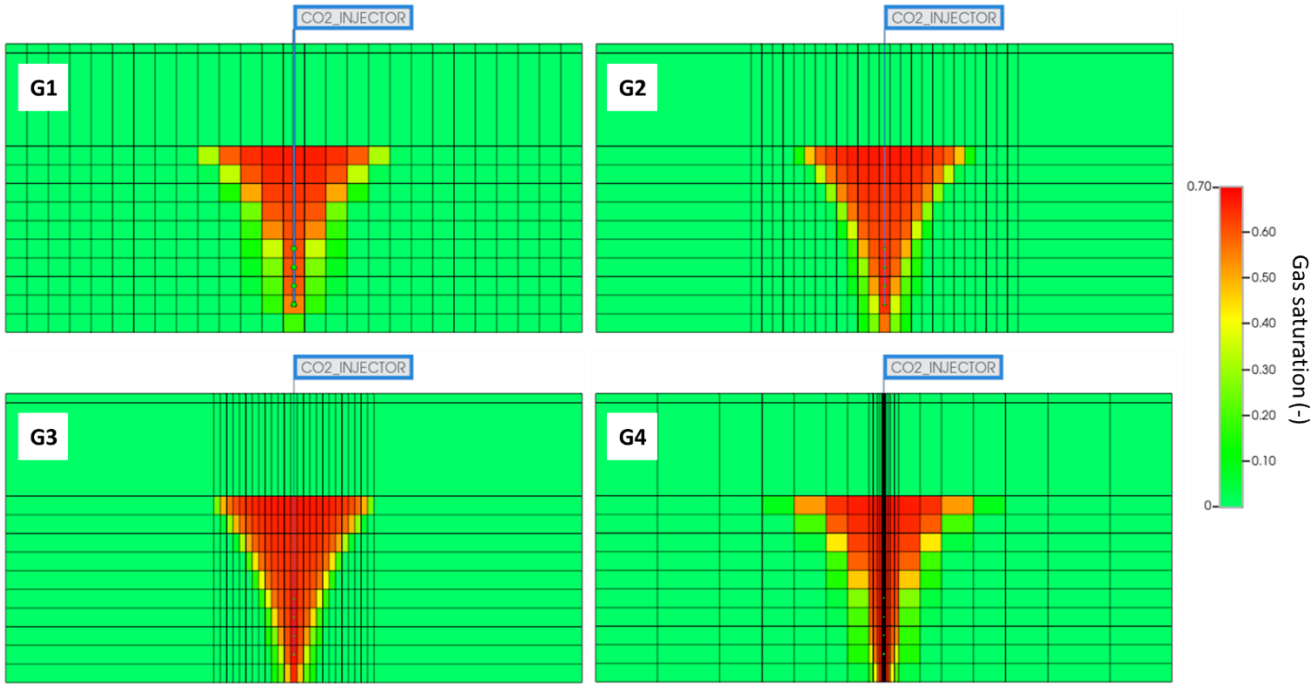

Figure 22 *Gas saturation after injection for different gridding in GEM (IK 2D view)*

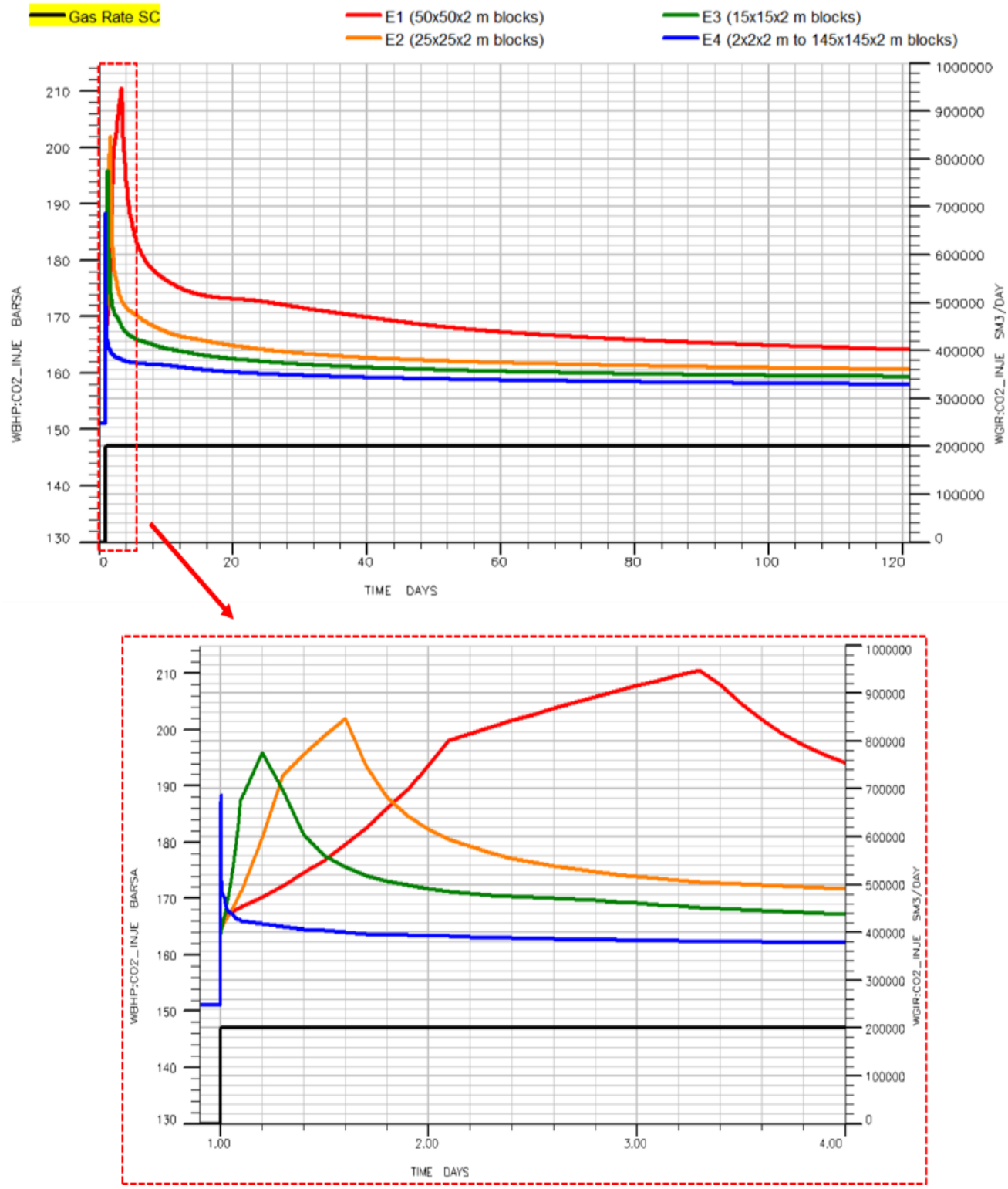

Figure 23 *Well bottom-hole pressure profiles for grids E1, E2, E3 and E4*

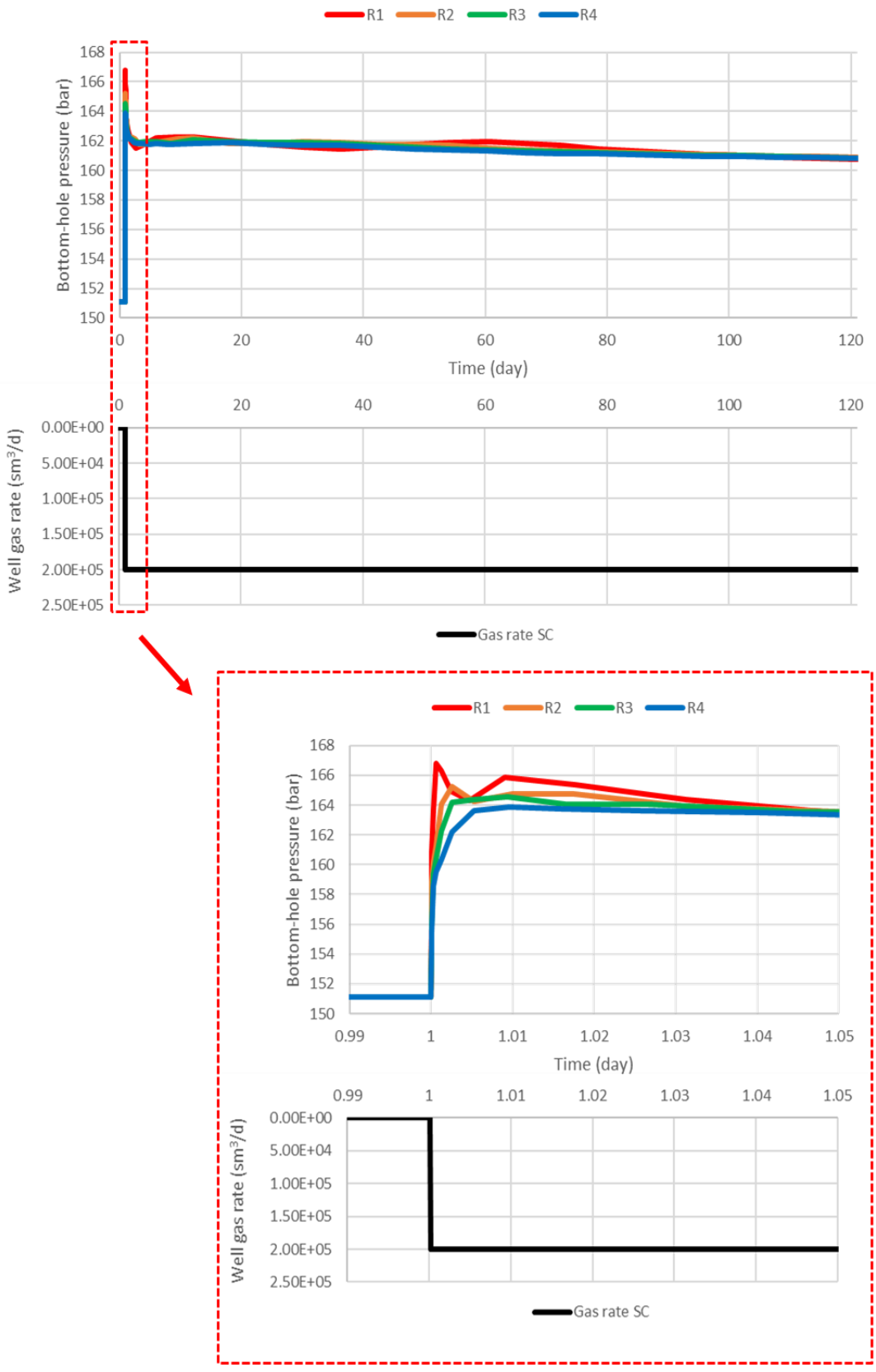

Figure 24 *Well bottom-hole pressure profiles for the grids R1, R2, R3 and R4*

4.2 Ramp-up injection scenarios

Ideally, a very refined grid should be used to correctly model the pressure trend during injection. However, considering that a number of injector wells would be typically simulated in a full reservoir study, the need for grid refinement might significantly increase the number of grid blocks thus also dramatically increase the simulation run time and/or the computational requirements.

A good strategy to compromise between grid refinement and the fictitious local pressure increase at the wellbore can be to inject CO_2 according to a rate ramp-up. To this end, three scenarios were simulated. Each scenario consisted in ramping the rate up to the original value of 200,000 sm^3/day with a different duration and increase of the subsequent rate steps. The three ramp-up scenarios are reported in Table 10 along with the corresponding values of the maximum well bottom-hole pressure and of the well bottom-hole pressure after injection. The results show that a ramp-up injection rate can effectively mitigate the non-physical well pressure increase and also that a progressive convergence between the maximum well bottom-hole pressure and the final aquifer overpressure after injection is obtained. The results are also shown in Figure 25.

Table 10 *Ramp-up injection scenarios*

Scenario	**ORIGINAL**	**1**	**2**	**3**
Steps	1	2	4	8
Time step (days)	120	60	30	15
Rate step (sm^3/day)	200000	100000	50000	25000
GRID G1				
Maximum well bottom-hole pressure (bar)	188.4	170.2	165.4	164.5
Maximum well bottom-hole overpressure (bar)	37.3	19.1	14.3	13.5
Well bottom-hole pressure after injection (bar)	162.5	162.8	163.4	163.9
GRID G2				
Maximum well bottom-hole pressure (bar)	184.6	168.3	161.6	161.5
Maximum well bottom-hole overpressure (bar)	33.5	17.2	10.5	10.4
Well bottom-hole pressure after injection (bar)	161.1	161.3	161.4	161.5
GRID G3				
Maximum well bottom-hole pressure (bar)	182.3	167.2	161.1	161.1
Maximum well bottom-hole overpressure (bar)	31.2	16.1	10.0	10.0
Well bottom-hole pressure after injection (bar)	160.8	160.9	161.0	161.1
GRID G4				
Maximum well bottom-hole pressure (bar)	170.6	163.4	160.6	160.6
Maximum well bottom-hole overpressure (bar)	19.5	12.3	9.5	9.5
Well bottom-hole pressure after injection (bar)	160.5	160.6	160.6	160.6

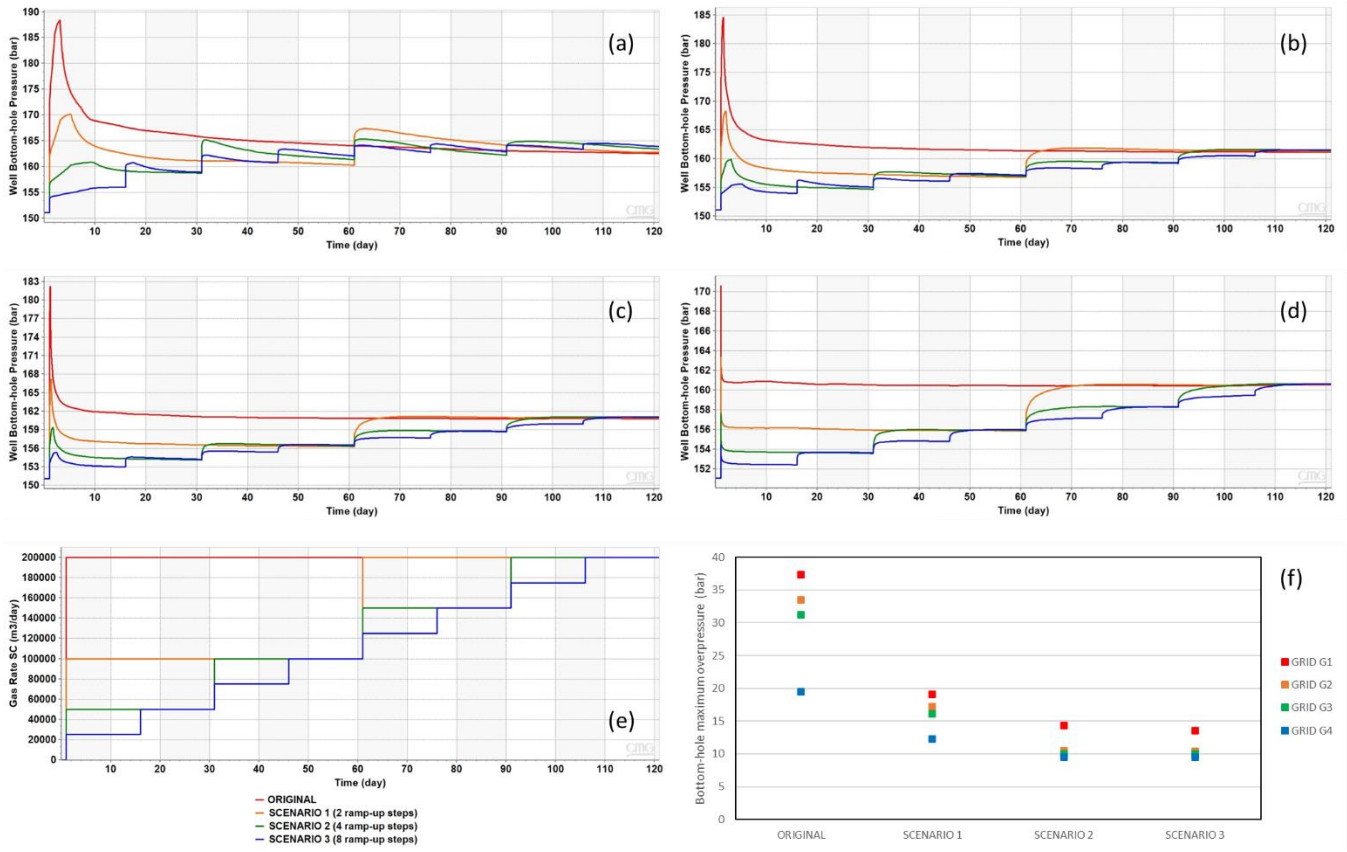

Figure 25 *Well bottom-hole pressure profiles for the grids (a) G1, (b) G2, (c) G3 and (d) G4 for ramp-up injection scenarios 1, 2 and 3; (e) Well gas rate SC for ramp-up injection scenarios 1, 2, 3; (f) Well bottom-hole maximum overpressure for the grids G1, G2, G3 and G4 for ramp-up injection scenarios 1, 2 and 3*

4.3 Gridding effects on CO_2 solubility and residual trapping

Grid discretization also proved to strongly affect CO_2 trapping. Simulations were performed for monitoring periods of 100, 200, 500 years, respectively, after injection. The three monitoring periods were defined so as to validate the obtained results.

As expected, stratigraphic/hydrodynamic trapping does not depend on gridding whereas mineral trapping does not concur to constrain the CO_2 underground in the short term. However, given that only a small volume of CO_2 was injected into the aquifer, all the CO_2 is either dissolved into the water or trapped by capillary forces some 100 years after injection. Results showed that the model discretization strongly affects solubility trapping and, consequently, residual trapping of the CO_2. A different trend is observed between these trapping mechanisms (Figure 26). The CO_2 immobilized by residual trapping decreases from the coarse grid to the fine grid (i.e., from G1 to G4) while an opposite trend is observed for solubility trapping. This translates into an average of 15% discrepancy between the trapped CO_2 by both residual and solubility trapping for monitoring periods of 100 and 200 years. After 500 years of simulation, CO_2 is almost completely dissolved into the brine for all the simulated grids, except for G1 in which 5% of CO_2 remains trapped by capillary forces. This is due to the supercritical CO_2-formation water interface surface, which is larger in fine grids compared to coarse grids; since supercritical CO_2 dissolves into the aqueous phase only at the CO_2-water interface, the solubility trapping of CO_2 is strongly dependent on

the extension of this interface [23]. The higher is the amount of CO_2 dissolved into the formation water the lower is the CO_2 which remains trapped as supercritical phase by residual trapping.

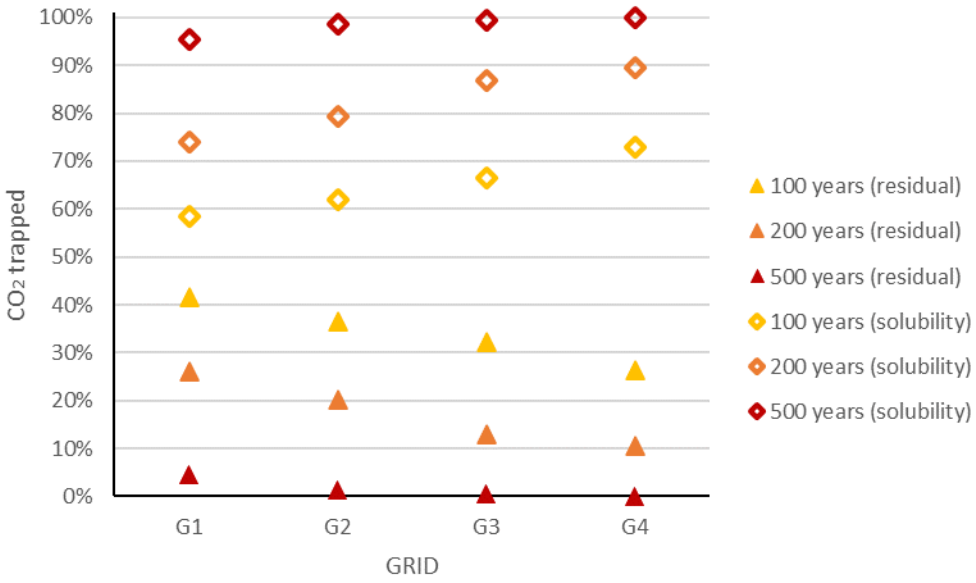

Figure 26 *Percentage of CO_2 trapped by residual and solubility trapping mechanisms for grids G1, G2, G3 and G4 after 100, 200 and 500 years, respectively*

4.4 Geochemistry sensitivities

Initial geochemical conditions resulted to be strongly responsible for how the injected CO_2 distributes among the different trapping mechanisms after 200 years of simulation. Table 11 shows the simulation results highlighting the minimum and the maximum CO_2 trapped quantity (as a percentage of the injected volume) due to each mechanism; results are also graphically represented in Figures 27 and 28.

GC1 proved to be the best scenario for hydrodynamic and the worst for residual trapping. Conversely, GC9 shows the lowest amount of CO_2 trapped by hydrodynamic trapping but the highest amount trapped as residual saturation. The discrepancy between hydrodynamic and residual trapping is some 6% and 8%, respectively and it is likely due to the effects caused by other trapping mechanisms. For example, the higher solubility trapping the lower is the supercritical CO_2 that can remain trapped as residual saturation.

Solubility trapping is strongly affected by geochemistry as well, and a discrepancy of about 4% is detected between scenarios GC9 and GC1. Scenario GC9 is characterized by the highest brine salinity while GC1 by the lowest one among the ones considered and thus, the observed discrepancy is in total agreement with the fact that CO_2 solubility in water decreases when water salinity increases [91].

The trend of ionic trapping mechanism is easy to understand: the higher the brine initial pH the higher the brine concentration of hydroxide ions and, as a consequence, the higher the quantity of CO_2 dissociated in the aqueous phase in the form of bicarbonate or carbonate according to reactions (2) and (3) discussed in section 1.3.

Metal cations availability in the brine highly influences mineral trapping and is responsible for a discrepancy of about 1.3% between scenario GC2 and GC7. As already observed for solubility trapping, the difference in brine salinity between these two scenarios is the main reason for mineral trapping discrepancy: the higher the cations availability the larger the quantity of solid carbonate minerals forming from CO_2 according to the reactions discussed in section 3.3.
In the investigated time frame, a negligible impact due to different initial mineral compositions on geochemical trapping mechanisms was detected (±0.3% in solubility and ±0.2% in ionic and mineral trapping).
Considering all the trapping mechanisms (Figure 28), the scenarios considering brine datasets A1 and A4 show a tendency to trap CO_2 by geochemical mechanisms; conversely, when datasets A2 and A3 are simulated hydrogeological trapping is favored. Scenarios adopting brine A1 are characterized by the highest quantity of CO_2 trapped by solubility because of the brine low salinity while the scenario using brine A4 is characterized by the highest ionic trapping because of the relatively high brine pH and by high mineral trapping because of the brine free cations' concentration.

Table 11 *CO_2 trapped by different mechanisms after 200 years according to geochemistry scenarios in GEM*

Geochemistry scenario	**GC1**	**GC2**	**GC3**	**GC4**	**GC5**	**GC6**	**GC7**	**GC8**	**GC9**	**GC10**	**GC11**	**GC12**
Brine dataset	A1			A2			A3			A4		
Mineralogy dataset	M1	M2	M3	M1	M2	M3	M1	M2	M3	M1	M2	M3
Hydrodynamic trapping (%)	20.48	18.26	19.05	17.95	18.84	18.72	14.89	14.79	14.52	18.21	18.84	19.34
Residual trapping (%)	52.74	55.81	54.62	57.87	56.66	56.84	60.10	60.25	60.77	56.25	55.08	54.36
Solubility trapping (%)	19.28	18.69	19.02	16.45	16.68	16.69	15.50	15.47	15.37	15.93	16.29	16.43
Ionic trapping (%)	0.537	0.526	0.531	0.599	0.603	0.603	1.461	1.458	1.460	1.792	1.814	1.828
Mineral trapping (%)	6.968	6.727	6.784	7.131	7.218	7.149	8.050	8.029	7.885	7.821	7.972	8.045
Hydrogeological trapping (%)	73.22	74.06	73.67	75.82	75.50	75.56	74.99	75.04	75.29	74.46	73.92	73.69
Geochemical trapping (%)	26.78	25.94	26.33	24.18	24.50	24.44	25.01	24.96	24.71	25.54	26.08	26.31

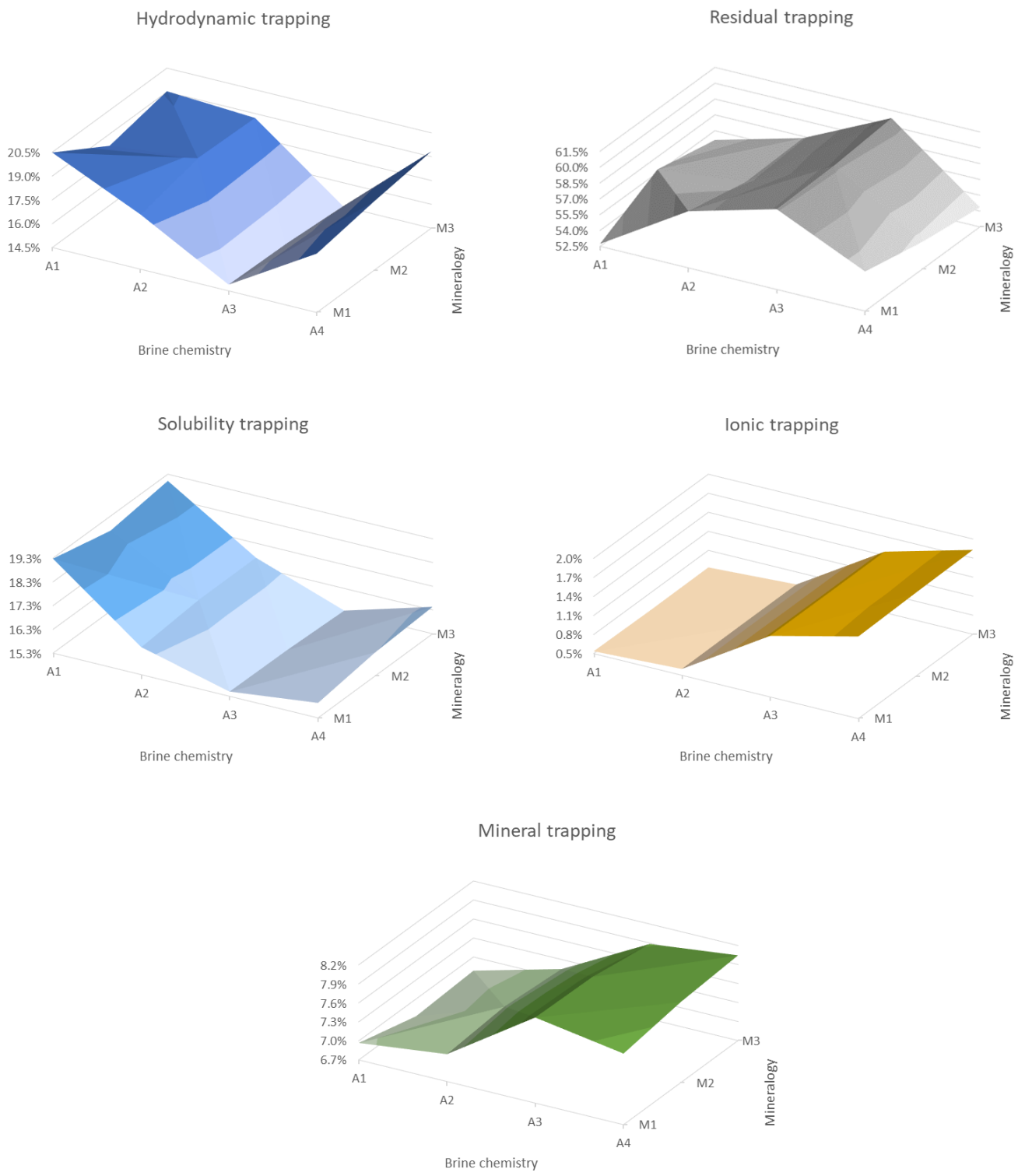

Figure 27 *CO_2 trapped by different mechanisms after 200 years according to geochemistry scenarios in GEM (part I)*

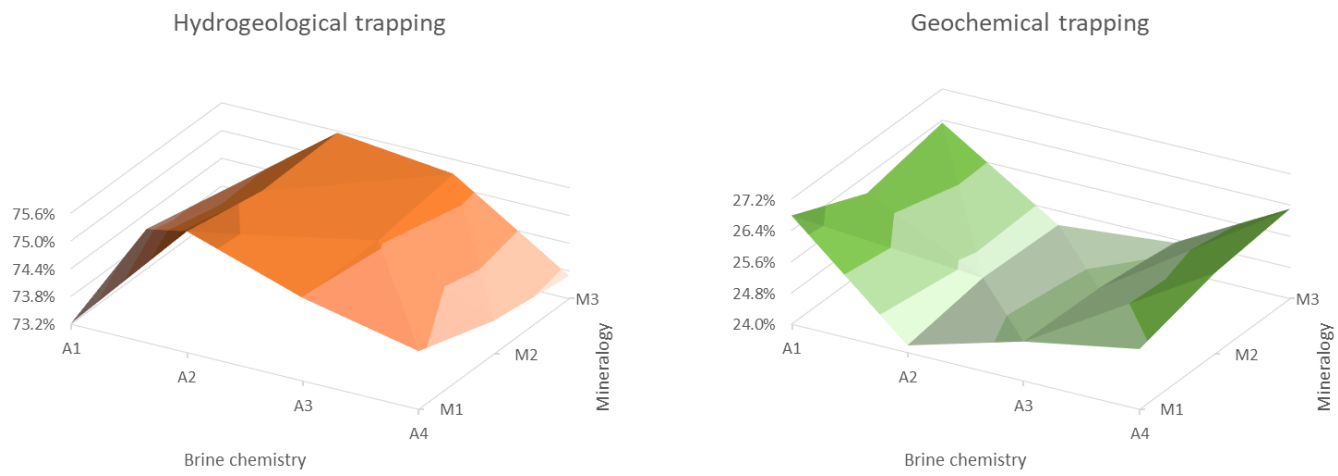

Figure 28 *CO_2 trapped by different mechanisms after 200 years according to geochemistry scenarios in GEM (part II)*

To better investigate how mineral composition affects various trapping mechanisms, simulations were repeated elapsing their duration to 1000 years. Considering the available brine chemistry dataset, simulations results offer outcomes similar to the ones observed at 200 years but the magnitude of each trapping mechanism and their discrepancies are of course different (Table 12) yet consistent with what discussed in section 1.4.

Eventually, longer simulations allow one to observe how the different mineralogy affects trapping mechanisms: taking the mineralogic composition M1 as a reference, mineral trapping decreases by 1.5% when mineralogy M3 is adopted (Figure 29). This result is justified by the fact that, according to the potential CO_2 fixed by each mineral taken by Rackley [25] (Figure 6), M1 mineralogy offers an average 76.22 kg/m^3 of potential fixed CO_2 while this value is 66.86 kg/m^3 for M2 and 57.03 kg/m^3 for M3.

The same discrepancy but to a lesser extent is observed for ionic trapping, decreasing by 0.15% from mineralogy M1 to M3, whereas solubility trapping increases by 0.6% from M1 to M3 confirming that the geochemical mechanism most influenced by mineralogy is mineral trapping. No clear pattern can be recognized for hydrodynamic and residual trapping among different mineralogy datasets but the whole geochemical trappings overall decrease by 1% from M1 to M3, while hydrogeological trapping does the opposite (Figures 29 and 30). As a consequence, M1 dataset offers the highest level of safety among the considered datasets.

According to the simulation results, due to carbonate minerals precipitation in the available pore volume, porosity slightly decreases.

As a last remark, taking into account all the considerations made in section 4.1, no CO_2 is detected above the caprock even after 1000 years of simulation.

Table 12 *CO_2 trapped by different mechanisms after 1000 years according to geochemistry scenarios GC1, GC2 and GC3 in GEM*

Geochemistry scenario	**GC1**	**GC2**	**GC3**
Brine dataset	A1		
Mineralogy dataset	M1	M2	M3
Hydrodynamic trapping (%)	12.62	10.40	11.67
Residual trapping (%)	46.70	49.60	48.68
Solubility trapping (%)	21.28	21.22	21.84
Ionic trapping (%)	0.946	0.893	0.799
Mineral trapping (%)	18.46	17.89	17.01
Hydrogeological trapping (%)	59.31	59.99	60.34
Geochemical trapping (%)	40.69	40.01	39.66

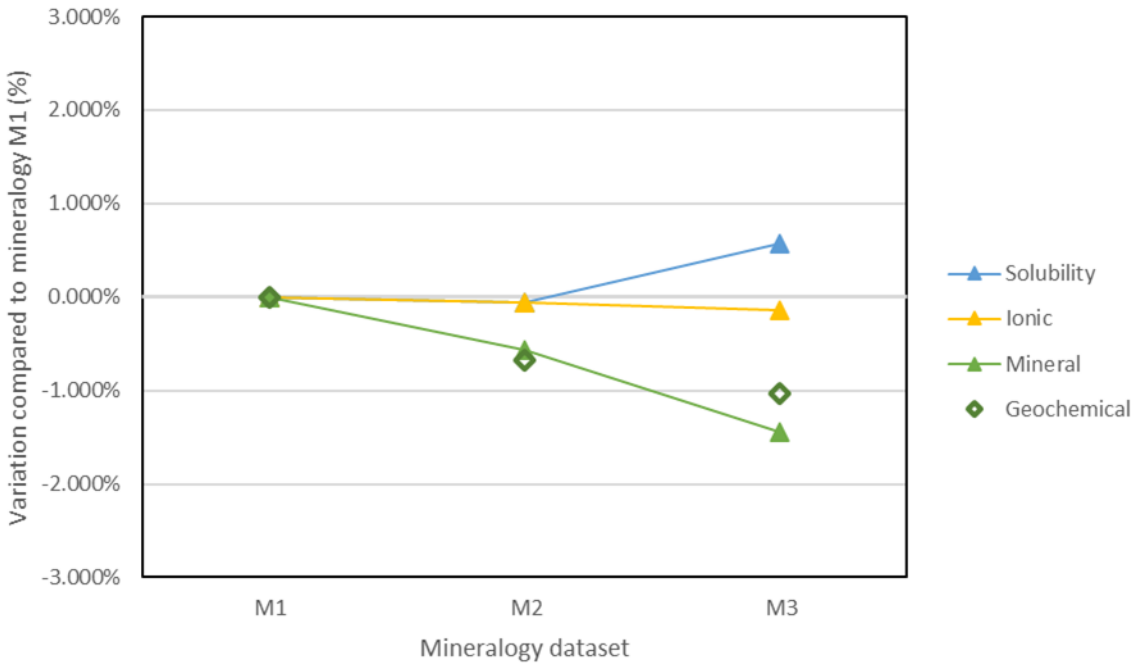

Figure 29 *Percentage variation of CO_2 trapped by geochemical mechanisms after 1000 years compared to mineralogy M1 in GEM*

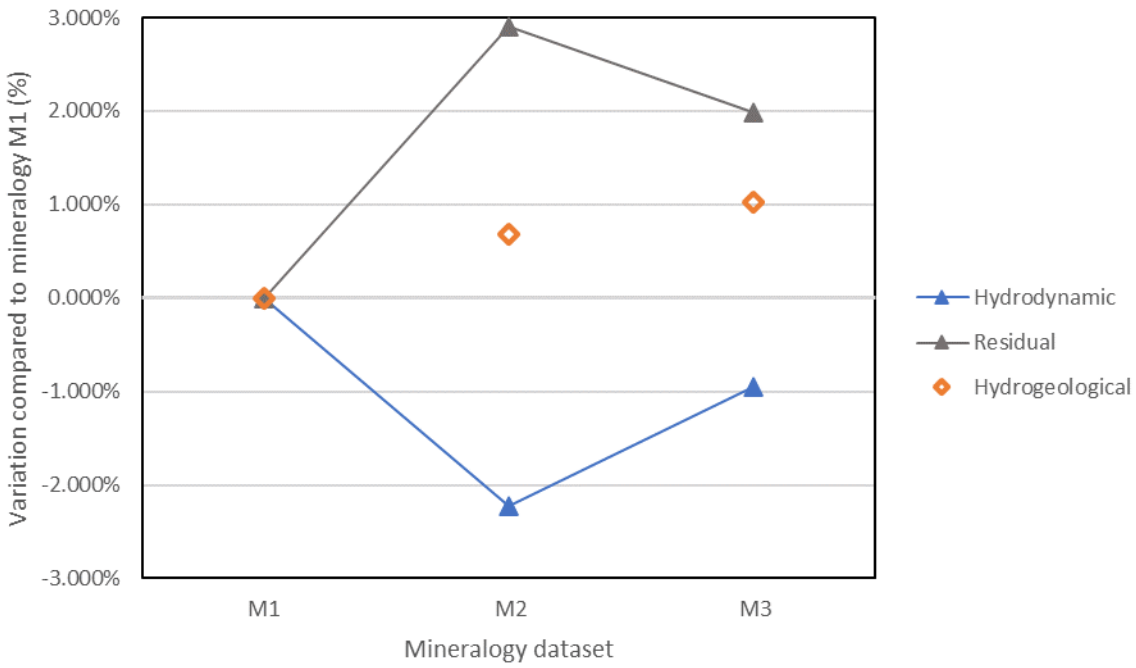

Figure 30 *Percentage variation of CO2 trapped by hydrogeological mechanisms after 1000 years compared to mineralogy M1 in GEM*

5. Conclusions

According to the results obtained in this thesis, the following conclusions can be drawn:

- As expected, the model discretization used for simulating CO_2 injection into a deep saline aquifer has a strong impact on the well bottom-hole pressure. A coarse grid in the near-wellbore area generates an unrealistic bottom-hole pressure profile at the beginning of injection. In particular, a significant difference in the maximum overpressure value between a fine and a coarse grid is observed. The reason for this is that initially, there is no CO_2 in the aquifer (i.e. CO_2 saturation is zero) thus effective permeability is also null; the larger the grid blocks the larger volume of CO_2 needed to reach the critical saturation, and thus the higher the pressure. Even if to a slightly different extent, this phenomenon is well represented by all the software used for the simulations (CMG-GEM, ECLIPSE100 and Rubis). Based on the simulation results analyzed in terms of pressure induced by injection, it is reasonable to confirm that a fine grid provides more reliable results.
- When a set of injection strategies with a rate ramp-up is considered, much more limited maximum overpressure values at the well are observed. By increasing the number of rate steps and decreasing the rate increments, the fictious well bottom-hole pressure increase during early CO_2 injection can be avoided. Thus, a well-calibrated ramp-up injection strategy can be very efficient to obtain consistent simulation results without excessive grid refinement in the near wellbore area, which might be an issue due to the increase in the number of model grid blocks in the case of large models and multiple injectors.
- Grid discretization also impacts on the long-term simulation of CO_2 storage since the amount of CO_2 trapped by residual and solubility trapping is highly affected by block dimensions. Smaller blocks lead to a higher quantity of CO_2 dissolved into the formation water and to a lower amount of CO_2 trapped by residual trapping. The discrepancy observed for the adopted grid discretization is about 15% for a simulated monitoring time of 100 and 200 years after injection. After 500 years of simulation, CO_2 is almost completely dissolved into brine for all the grids, except for the coarsest grid in which 5% of CO_2 remains trapped as residual saturation. Therefore, it can be affirmed that a coarse grid leads to an underestimation of the CO_2 trapped by solubility and to an overestimation of the CO_2 trapped by residual trapping. Even though mineral trapping was not simulated in this part of the study, because it typically occurs over very long timescale and it was beyond the scope of this study, it is evident that an underestimation of the CO_2 trapped by solubility will also lead to an underestimation of the quantity of mineralized CO_2.
- Sensitivities to rock geochemistry and brine properties using real datasets proved that brine has the strongest impact on the simulation results in terms of quantities of CO_2 trapped by different mechanisms in the relatively short term (hundreds of years). Higher salinity and free cations concentration result into higher mineral trapping while ionic trapping increases when brine pH increases. Conversely, solubility trapping decreases when salinity is high. When simulations are elapsed to 1000 years, the effects of the rock mineral composition become significant and can be detected: the higher the percentage of mineral reactants (K-feldspar, anorthite, chlorite…) the higher the CO_2 mineral trapping and thus the long-term safety of the storage.

References

[1] Benson, S.M., Surles, T., 2006. Carbon Dioxide Capture and Storage: An Overview With Emphasis on Capture and Storage in Deep Geological Formations. Proc. IEEE 94, 1795–1805. https://doi.org/10.1109/JPROC.2006.883718

[2] Rocca, V., Viberti, D., 2013. ENVIRONMENTAL SUSTAINABILITY OF OIL INDUSTRY. American Journal of Environmental Sciences 9, 210–217. https://doi.org/10.3844/ajessp.2013.210.217

[3] Bocchini, S., Castro, C., Cocuzza, M., Ferrero, S., Latini, G., Martis, A., Pirri, F., Scaltrito, L., Rocca, V., Verga, F., Viberti, D., 2017. The Virtuous CO_2 Circle or the Three Cs: Capture, Cache, and Convert. Journal of Nanomaterials 2017, 1–14. https://doi.org/10.1155/2017/6594151

[4] Alcalde, J., Flude, S., Wilkinson, M., Johnson, G., Edlmann, K., Bond, C.E., Scott, V., Gilfillan, S.M.V., Ogaya, X., Haszeldine, R.S., 2018. Estimating geological CO2 storage safety to deliver on climate mitigation. Nat Commun 9, 2201. https://doi.org/10.1038/s41467-018-04423-1

[5] Bui, M., Adjiman, C.S., Bardow, A., Anthony, E.J., Boston, A., Brown, S., Fennell, P.S., Fuss, S., Galindo, A., Hackett, L.A., Hallett, J.P., Herzog, H.J., Jackson, G., Kemper, J., Krevor, S., Maitland, G.C., Matuszewski, M., Metcalfe, I.S., Petit, C., Puxty, G., Reimer, J., Reiner, D.M., Rubin, E.S., Scott, S.A., Shah, N., Smit, B., Trusler, J.P.M., Webley, P., Wilcox, J., Mac Dowell, N., 2018. Carbon capture and storage (CCS): the way forward. Energy Environ. Sci. 11, 1062–1176. https://doi.org/10.1039/C7EE02342A

[6] Benetatos, C., Borello, E.S., Peter, C., Rocca, V., Romagnoli, R., 2019. Considerations on energy transition. GEAM 3, 26–31.

[7] Benetatos, C., Bocchini, S., Carpignano, A., Chiodoni, A., Cocuzza, M., Deangeli, C., Eid, C., Ferrero, D., Gerboni, R., Giglio, G., Lamberti, A., Marasso, S., Massimiani, A., Menin, B., Moscatello, A., Panini, F., Peter, C., Pirri, F., Quaglio, M., Rocca, V., Rovere, A., Borello, E.S., Serazio, C., Uggenti, A.C., Vasile, N., Verga, F., Viberti, D., 2021. How underground systems can contribute to meet the challenges of energy transition. GEAM-2021-163-164-163-164 1224, 65–80. https://doi.org/10.19199/2021.163-164.1121-9041.065

[8] Kalam, S., Olayiwola, T., Al-Rubaii, M.M., Amaechi, B.I., Jamal, M.S., Awotunde, A.A., 2021. Carbon dioxide sequestration in underground formations: review of experimental, modeling, and field studies. J Petrol Explor Prod Technol 11, 303–325. https://doi.org/10.1007/s13202-020-01028-7

[9] IEA, 2021. Net Zero by 2050 - A Roadmap for the Global Energy Sector.

[10] Celia, M.A., Bachu, S., Nordbotten, J.M., Bandilla, K.W., 2015. Status of CO_2 storage in deep saline aquifers with emphasis on modeling approaches and practical simulations: STATUS OF CO_2 STORAGE IN DEEP SALINE AQUIFERS. Water Resour. Res. 51, 6846–6892. https://doi.org/10.1002/2015WR017609

[11] Vangkilde-Pedersen, T., Anthonsen, K.L., Smith, N., Kirk, K., neele, F., van der Meer, B., Le Gallo, Y., Bossie-Codreanu, D., Wojcicki, A., Le Nindre, Y.-M., Hendriks, C., Dalhoff, F., Peter Christensen, N., 2009. Assessing European capacity for geological storage of carbon dioxide–the EU GeoCapacity project. Energy Procedia 1, 2663–2670. https://doi.org/10.1016/j.egypro.2009.02.034

[12] Delprat-Jannaud, F., Korre, A., Shi, J.Q., McConnell, B., Arvanitis, A., Boavida, D., Car, M., Gastine, M., Grunnaleite, I., Bateman, K., Poulsen, N., Sinayuc, C., Vähäkuopus, T., Vercelli, S., Wójcicki, A., 2013. State-of-the-art review of CO2 Storage Site Selection and Characterisation Methods (No. D3.3). CGS Europe.

[13] IPCC Special Report on Carbon Dioxide Capture and Storage. Prepared by Working Group III of the Intergovernmental Panel on Climate Change [Metz, B., O. Davidson, H. C. de Coninck, M. Loos, and L. A. Meyer (eds.)]. 2005, Cambridge University Press, Cambridge, United Kingdom and New York, NY, USA, 442 pp.

[14] Rochelle, C.A., Czernichowski-Lauriol, I., Milodowski, A.E., 2004. The impact of chemical reactions on CO2 storage in geological formations: a brief review. SP 233, 87–106. https://doi.org/10.1144/GSL.SP.2004.233.01.07

[15] Jun, Y.-S., Giammar, D.E., Werth, C.J., 2013. Impacts of Geochemical Reactions on Geologic Carbon Sequestration. Environ. Sci. Technol. 47, 3–8. https://doi.org/10.1021/es3027133

[16] Raza, A., Gholami, R., Rezaee, R., Rasouli, V., Rabiei, M., 2019. Significant aspects of carbon capture and storage – A review. Petroleum 5, 335–340. https://doi.org/10.1016/j.petlm.2018.12.007

[17] Gündoğan, Ö., 2011. Geochemical Modelling of CO2 Storage (PhD in Petroleum Engineering). Institute of Petroleum Engineering, Heriot-Watt University.

[18] Song, J., Zhang, D., 2013. Comprehensive Review of Caprock-Sealing Mechanisms for Geologic Carbon Sequestration. Environ. Sci. Technol. 47, 9–22. https://doi.org/10.1021/es301610p

[19] Rackley, S.A., 2017. Introduction to geological storage, in: Carbon Capture and Storage. Elsevier, pp. 285–304. https://doi.org/10.1016/B978-0-12-812041-5.00011-8

[20] Land, C.S., 1968. Calculation of Imbibition Relative Permeability for Two- and Three-Phase Flow from Rock Properties. Society of Petroleum Engineers Journal 8, 149–156. https://doi.org/10.2118/1942-PA

[21] Carlson, F.M., 1981. Simulation of Relative Permeability Hysteresis to the Nonwetting Phase. Presented at the SPE Annual Technical Conference and Exhibition, OnePetro. https://doi.org/10.2118/10157-MS

[22] Aissaoui, A., 1983. Theoretical and experimental study of capillary pressure hysteresis and relative permeability for natural gas underground storage. Ecole des Mines de Paris.

[23] Zhang, D., Song, J., 2014. Mechanisms for Geological Carbon Sequestration. Procedia IUTAM 10, 319–327. https://doi.org/10.1016/j.piutam.2014.01.027

[24] Gunter, W.D., Bachu, S., Benson, S., 2004. The role of hydrogeological and geochemical trapping in sedimentary basins for secure geological storage of carbon dioxide. SP 233, 129–145. https://doi.org/10.1144/GSL.SP.2004.233.01.09

[25] Rackley, S.A., 2017. Geochemical and biogeochemical features, events, and processes, in: Carbon Capture and Storage. Elsevier, pp. 365–386. https://doi.org/10.1016/B978-0-12-812041-5.00014-3

[26] Han, W.S., McPherson, B.J., Lichtner, P.C., Wang, F.P., 2010. Evaluation of trapping mechanisms in geologic CO2 sequestration: Case study of SACROC northern platform, a 35-year CO2 injection site. American Journal of Science 310, 282–324. https://doi.org/10.2475/04.2010.03

[27] Ajayi, T., Gomes, J.S., Bera, A., 2019. A review of CO2 storage in geological formations emphasizing modeling, monitoring and capacity estimation approaches. Pet. Sci. 16, 1028–1063. https://doi.org/10.1007/s12182-019-0340-8

[28] Szulczewski, M.L., MacMinn, C.W., Herzog, H.J., Juanes, R., 2012. Lifetime of carbon capture and storage as a climate-change mitigation technology. Proc. Natl. Acad. Sci. U.S.A. 109, 5185–5189. https://doi.org/10.1073/pnas.1115347109

[29] Ghaderi, S.M., Keith, D.W., Leonenko, Y., 2009. Feasibility of Injecting Large Volumes of CO2 into Aquifers. Energy Procedia 1, 3113–3120. https://doi.org/10.1016/j.egypro.2009.02.092

[30] Miri, R., Hellevang, H., 2016. Salt precipitation during CO 2 storage—A review. International Journal of Greenhouse Gas Control 51, 136–147. https://doi.org/10.1016/j.ijggc.2016.05.015

[31] Miri, R., Hellevang, H., n.d. FME SUCCESS Synthesis report Volume 3.

[32] Cui, G., Ren, S., Zhang, L., Ren, B., Zhuang, Y., Li, X., Han, B., Zhang, P., 2016. Formation water evaporation induced salt precipitation and its effect on gas production in high temperature natural gas reservoirs. Petroleum Exploration and Development 43, 815–824. https://doi.org/10.1016/S1876-3804(16)30097-0

[33] Tang, Y., Yang, R., Kang, X., 2018. Modeling the effect of water vaporization and salt precipitation on reservoir properties due to carbon dioxide sequestration in a depleted gas reservoir. Petroleum 4, 385–397. https://doi.org/10.1016/j.petlm.2017.12.003

[34] Gollakota, S., McDonald, S., 2014. Commercial-scale CCS Project in Decatur, Illinois – Construction Status and Operational Plans for Demonstration. Energy Procedia 63, 5986–5993. https://doi.org/10.1016/j.egypro.2014.11.633

[35] Streibel, M., Finley, R.J., Martens, S., Greenberg, S., Möller, F., Liebscher, A., 2014. From Pilot to Demo Scale – Comparing Ketzin results with the Illinois Basin-decatur Project. Energy Procedia 63, 6323–6334. https://doi.org/10.1016/j.egypro.2014.11.665

[36] Aquistore Project, a Deep Saline CO2 Storage Demonstration Project, 2013. Natural Resources Canada.

[37] Aquistore: CO2 storage at the world's first integrated CCS project. Project summary report., 2015. Global Carbon Capture and Storage Institute Ltd.

[38] The Quest for less CO2: learning from CCS implementation in Canada. A case study on Shell's Quest CCS Project, 2015. Shell.

[39] Rock, L., O'Brien, S., Tessarolo, S., Duer, J., Bacci, V.O., Hirst, B., Randell, D., Helmy, M., Blackmore, J., Duong, C., Halladay, A., Smith, N., Dixit, T., Kassam, S., Yaychuk, M., 2017. The Quest CCS Project: 1st Year Review Post Start of Injection. Energy Procedia 114, 5320–5328. https://doi.org/10.1016/j.egypro.2017.03.1654

[40] Alcade, J., Flude, S., 2020. Carbon capture and storage has stalled needlessly – three reasons why fears of CO_2 leakage are overblown [WWW Document]. The Conversation. URL http://theconversation.com/carbon-capture-and-storage-has-stalled-needlessly-three-reasons-why-fears-of-co-leakage-are-overblown-130747 (accessed 9.17.22).

[41] Bachu, S., 2016. Identification of oil reservoirs suitable for CO2-EOR and CO2 storage (CCUS) using reserves databases, with application to Alberta, Canada. International Journal of Greenhouse Gas Control 44, 152–165. https://doi.org/10.1016/j.ijggc.2015.11.013

[42] Eshraghi, S.E., Rasaei, M.R., Zendehboudi, S., 2016. Optimization of miscible CO2 EOR and storage using heuristic methods combined with capacitance/resistance and Gentil fractional flow models. Journal of Natural Gas Science and Engineering 32, 304–318. https://doi.org/10.1016/j.jngse.2016.04.012

[43] Eide, L.I., Batum, M., Dixon, T., Elamin, Z., Graue, A., Hagen, S., Hovorka, S., Nazarian, B., Nøkleby, P.H., Olsen, G.I., Ringrose, P., Vieira, R.A.M., 2019. Enabling Large-Scale Carbon Capture, Utilisation, and Storage (CCUS) Using Offshore Carbon Dioxide (CO2) Infrastructure Developments—A Review. Energies 12, 1945. https://doi.org/10.3390/en12101945

[44] Cui, G., Zhu, L., Zhou, Q., Ren, S., Wang, J., 2021. Geochemical reactions and their effect on CO2 storage efficiency during the whole process of CO2 EOR and subsequent storage. International Journal of Greenhouse Gas Control 108, 103335. https://doi.org/10.1016/j.ijggc.2021.103335

[45] Young-Lorenz, J.D., 2013. PORTFOLIO ANALYSIS OF CARBON SEQUESTRATION TECHNOLOGIES AND BARRIERS TO ADOPTION (Master of Science in Geoscience). University of Western Australia.

[46] Oldenburg, C.M., 2007. Joule-Thomson cooling due to CO2 injection into natural gas reservoirs. Energy Conversion and Management 48, 1808–1815. https://doi.org/10.1016/j.enconman.2007.01.010

[47] Gao, M., Wang, L., Chen, X., Wei, X., Liang, J., Li, L., 2021. Joule–Thomson Effect on a CCS-Relevant (CO_2 + N_2) System. ACS Omega 6, 9857–9867. https://doi.org/10.1021/acsomega.1c00554

[48] Gor, G.Yu., Prévost, J.H., 2013. Effect of CO2 Injection Temperature on Caprock Stability. Energy Procedia 37, 3727–3732. https://doi.org/10.1016/j.egypro.2013.06.267

[49] André, L., Azaroual, M., Menjoz, A., 2010. Numerical Simulations of the Thermal Impact of Supercritical CO2 Injection on Chemical Reactivity in a Carbonate Saline Reservoir. Transp Porous Med 82, 247–274. https://doi.org/10.1007/s11242-009-9474-2

[50] Porthos Carbon Capture and Storage Project, Rotterdam, Netherlands, n.d. . NS Energy. URL https://www.nsenergybusiness.com/projects/porthos-carbon-capture-and-storage-ccs-project/ (accessed 9.13.22).

[51] Furre, A.-K., Eiken, O., Alnes, H., Vevatne, J.N., Kiær, A.F., 2017. 20 Years of Monitoring CO2-injection at Sleipner. Energy Procedia 114, 3916–3926. https://doi.org/10.1016/j.egypro.2017.03.1523

[52] Wright, I., 2006. CO2 Geological Storage: Lesson Learned from In Salah (Algeria). Presented at the SBSTA Meeting Bonn, Bonn.

[53] Haddadji, R., 2006. The In-Salah CCS experience Sonatrach, Algeria. Presented at the The First International Conference on the Clean The First International Conference on the Clean Development Mechanism, Riyadh, Saudi Arabia.

[54] Ringrose, P.S., Mathieson, A.S., Wright, I.W., Selama, F., Hansen, O., Bissell, R., Saoula, N., Midgley, J., 2013. The In Salah CO2 Storage Project: Lessons Learned and Knowledge Transfer. Energy Procedia 37, 6226–6236. https://doi.org/10.1016/j.egypro.2013.06.551

[55] Balch, R., McPherson, B., 2016. Integrating Enhanced Oil Recovery and Carbon Capture and Storage Projects: A Case Study at Farnsworth Field, Texas, in: All Days. Presented at the SPE Western Regional Meeting, SPE, Anchorage, Alaska, USA, p. SPE-180408-MS. https://doi.org/10.2118/180408-MS

[56] Preston, C., Monea, M., Jazrawi, W., Brown, K., Whittaker, S., White, D., Law, D., Chalaturnyk, R., Rostron, B., 2005. IEA GHG Weyburn CO2 monitoring and storage project. Fuel Processing Technology 86, 1547–1568. https://doi.org/10.1016/j.fuproc.2005.01.019

[57] Prévost, J.H., Fuller, R., Altevogt, A.S., Bruant, R., Scherer, G., 2005. - Numerical modeling of carbon dioxide injection and transport in Deep Saline Aquifers, in: Rubin, E.S., Keith, D.W., Gilboy, C.F., Wilson, M., Morris, T., Gale, J., Thambimuthu, K. (Eds.), Greenhouse Gas Control Technologies 7. Elsevier Science Ltd, Oxford, pp. 2189–2193. https://doi.org/10.1016/B978-008044704-9/50298-6

[58] Ghanbari, S., Al-Zaabi, Y., Pickup, G.E., Mackay, E., Gozalpour, F., Todd, A.C., 2006. Simulation of CO2 Storage In Saline Aquifers. Chemical Engineering Research and Design, Carbon Capture and Storage 84, 764–775. https://doi.org/10.1205/cherd06007

[59] Ukaegbu, C., Gundogan, O., Mackay, E., Pickup, G., Todd, A., Gozalpour, F., 2009. Simulation of CO_2 storage in a heterogeneous aquifer. Proceedings of the Institution of Mechanical Engineers, Part A: Journal of Power and Energy 223, 249–267. https://doi.org/10.1243/09576509JPE627

[60] Juanes, R., Spiteri, E.J., Orr, F.M., Blunt, M.J., 2006. Impact of relative permeability hysteresis on geological CO_2 storage: IMPACT OF HYSTERESIS ON GEOLOGICAL CO_2 STORAGE. Water Resour. Res. 42. https://doi.org/10.1029/2005WR004806

[61] Pruess, K., Xu, T., Apps, J., Garcia, J., 2003. Numerical Modeling of Aquifer Disposal of CO2. SPE Journal 8, 49–60.

[62] Jobard, E., Sterpenich, J., Pironon, J., Corvisier, J., Randi, A., 2018. Experimental Modelling of the Caprock/Cement Interface Behaviour under CO2 Storage Conditions: Effect of Water and Supercritical CO2 from a Cathodoluminescence Study. Geosciences 8, 185. https://doi.org/10.3390/geosciences8050185

[63] Kumar, N., Bryant, S.L., 2008. Optimizing Injection Intervals in Vertical and Horizontal Wells for CO2 Sequestration, in: All Days. Presented at the SPE Annual Technical Conference and Exhibition, SPE, Denver, Colorado, USA. https://doi.org/10.2118/116661-MS

[64] Li, P., Liu, X., Lu, J., Zhou, D., Hovorka, S.D., Hu, G., Liang, X., 2018. Potential evaluation of CO_2 EOR and storage in oilfields of the Pearl River Mouth Basin, northern South China Sea: Original

Research Article: Potential evaluation of CO_2 EOR and storage in oilfields of the Pearl River Mouth Basin. Greenhouse Gas Sci Technol 8, 954–977. https://doi.org/10.1002/ghg.1808

[65] Khudaida, K.J., Das, D.B., 2020. A Numerical Analysis of the Effects of Supercritical CO2 Injection on CO2 Storage Capacities of Geological Formations. Clean Technol. 2, 333–364. https://doi.org/10.3390/cleantechnol2030021

[66] Urych, T., Chećko, J., Magdziarczyk, M., Smoliński, A., 2022. Numerical Simulations of Carbon Dioxide Storage in Selected Geological Structures in North-Western Poland. Front. Energy Res. 10, 827794. https://doi.org/10.3389/fenrg.2022.827794

[67] Arif, M., Al-Yaseri, A.Z., Barifcani, A., Lebedev, M., Iglauer, S., 2016. Impact of pressure and temperature on CO2–brine–mica contact angles and CO2–brine interfacial tension: Implications for carbon geo-sequestration. Journal of Colloid and Interface Science 462, 208–215. https://doi.org/10.1016/j.jcis.2015.09.076

[68] Al-Khdheeawi, E.A., Vialle, S., Barifcani, A., Sarmadivaleh, M., Iglauer, S., 2017. Influence of injection well configuration and rock wettability on CO2 plume behaviour and CO2 trapping capacity in heterogeneous reservoirs. Journal of Natural Gas Science and Engineering 43, 190–206. https://doi.org/10.1016/j.jngse.2017.03.016

[69] Ali, M., Aftab, A., Arain, Z.-U.-A., Al-Yaseri, A., Roshan, H., Saeedi, A., Iglauer, S., Sarmadivaleh, M., 2020. Influence of Organic Acid Concentration on Wettability Alteration of Cap-Rock: Implications for CO2 Trapping/Storage. ACS Appl. Mater. Interfaces 12, 39850–39858. https://doi.org/10.1021/acsami.0c10491

[70] Pentland, C.H., El-Maghraby, R., Georgiadis, A., Iglauer, S., Blunt, M.J., 2011. Immiscible Displacements and Capillary Trapping in CO2 Storage. Energy Procedia 4, 4969–4976. https://doi.org/10.1016/j.egypro.2011.02.467

[71] Iglauer, S., 2011. Dissolution Trapping of Carbon Dioxide in Reservoir Formation Brine – A Carbon Storage Mechanism, Mass Transfer - Advanced Aspects. IntechOpen. https://doi.org/10.5772/20206

[72] Golding, S.D., Uysal, I.T., Boreham, C.J., Kirste, D., Baublys, K.A., Esterle, J.S., 2011. Adsorption and mineral trapping dominate CO2 storage in coal systems. Energy Procedia 4, 3131–3138. https://doi.org/10.1016/j.egypro.2011.02.227

[73] Al-Khdheeawi, E.A., Mahdi, D.S., Ali, M., Fauziah, C.A., Barifcani, A., 2020. Impact of Caprock Type on Geochemical Reactivity and Mineral Trapping Efficiency of CO2, in: Day 1 Mon, November 02, 2020. Presented at the Offshore Technology Conference Asia, OTC, Kuala Lumpur, Malaysia, p. D012S001R060. https://doi.org/10.4043/30094-MS

[74] Coats, K.H., Thomas, L.K., Pierson, R.G., 1995. Compositional and Black Oil Reservoir Simulation. Presented at the 13th SPE Symposium on Reservoir Simulation, SPE, San Antonio, Texas, USA, p. 14.

[75] Gorrell, H.A., 1958. Classification of Formation Waters Based on Sodium Chloride Content: GEOLOGICAL NOTES. Bulletin 42. https://doi.org/10.1306/0BDA5BE8-16BD-11D7-8645000102C1865D

[76] Churcher, P.L., French, P.R., Shaw, J.C., Shramm, L.L., 1991. Rock Properties of Berea Sandstone, Baker Dolomite, and Indiana Limestone. Presented at the SPE International Symposium on Oilfield Chemistry, SPE, Anaheim, California, p. 19.

[77] Donnez, P., 2012. Essentials of Reservoir Engineering. Editions TECHNIP.

[78] Dullien, F.A.L., 2012. Porous Media: Fluid Transport and Pore Structure. Academic Press.

[79] Gershenzon, N.I., Ritzi, R.W., Dominic, D.F., Mehnert, E., Okwen, R.T., 2017. Capillary trapping of CO2 in heterogeneous reservoirs during the injection period. International Journal of Greenhouse Gas Control 59, 13–23. https://doi.org/10.1016/j.ijggc.2017.02.002

[80] Krevor, S.C.M., Pini, R., Zuo, L., Benson, S.M., 2012. Relative permeability and trapping of CO_2 and water in sandstone rocks at reservoir conditions: MULTIPHASE FLOW OF CO_2 AND WATER IN SANDSTONE ROCKS. Water Resour. Res. 48. https://doi.org/10.1029/2011WR010859

[81] Burnside, N.M., Naylor, M., 2014. Review and implications of relative permeability of CO2/brine systems and residual trapping of CO2. International Journal of Greenhouse Gas Control 23, 1–11. https://doi.org/10.1016/j.ijggc.2014.01.013

[82] Pini, R., Benson, S.M., 2017. Capillary pressure heterogeneity and hysteresis for the supercritical CO2/water system in a sandstone. Advances in Water Resources 108, 277–292. https://doi.org/10.1016/j.advwatres.2017.08.011

[83] Wijaya, Z., 2006. CO2 Injection in an Oil Reservoir with Gas Cap (Compositional Simulation Case at Heidrun Field Norway). NTNU, Trondheim, Norway.

[84] Yu, W., Zhang, Y., Varavei, A., Sepehrnoori, K., Zhang, T., Wu, K., Miao, J., 2019. Compositional Simulation of CO2 Huff 'n' Puff in Eagle Ford Tight Oil Reservoirs With CO2 Molecular Diffusion, Nanopore Confinement, and Complex Natural Fractures. SPE Reservoir Evaluation & Engineering 22, 492–508. https://doi.org/10.2118/190325-PA

[85] Peng, D.-Y., Robinson, D.B., 1976. A New Two-Constant Equation of State. Ind. Eng. Chem. Fund. 15, 59–64. https://doi.org/10.1021/i160057a011

[86] Harvey, A.H., 1996. Semiempirical correlation for Henry's constants over large temperature ranges. AIChE J. 42, 1491–1494. https://doi.org/10.1002/aic.690420531

[87] Wolery, T.J., 1992. EQ3/6, a software package for geochemical modeling of aqueous systems: Package overview and installation guide (Version 7.0) (No. UCRL-MA--110662-Pt.1, 138894). https://doi.org/10.2172/138894

[88] Nghiem, L., Sammon, P., Grabenstetter, J., Ohkuma, H., 2004. Modeling CO2 Storage in Aquifers with a Fully-Coupled Geochemical EOS Compositional Simulator. Presented at the SPE/DOE Fourteenth Symposium on Improved Oil Recovery, SPE, Tulsa, Oklahoma, USA, p. 16.

[89] Civan, F., 2000. Chapter 13: Inorganic Scaling and Geochemical formation damage, in: Reservoir Formation Damage: Fundamentals, Modeling, Assessment, and Mitigation. Gulf Publishing Company, Houston, Texas, USA, pp. 407–467.

[90] Xu, T., Spycher, N., Sonnenthal, E., Zhang, G., Zheng, L., Pruess, K., 2011. TOUGHREACT Version 2.0: A simulator for subsurface reactive transport under non-isothermal multiphase flow conditions. Computers & Geosciences 37, 763–774. https://doi.org/10.1016/j.cageo.2010.10.007

[91] Zhang, Y., Lashgari, H.R., Sepehrnoori, K., Di, Y., 2017. Effect of capillary pressure and salinity on CO2 solubility in brine aquifers. International Journal of Greenhouse Gas Control 57, 26–33. https://doi.org/10.1016/j.ijggc.2016.12.012